Modeling of the Film Blowing Process by using Variational Principles

Roman Kolařík

Bachelor Thesis
2006

Tomas Bata University in Zlín
Faculty of Technology

Univerzita Tomáše Bati ve Zlíně
Fakulta technologická
Ústav výrobního inženýrství
akademický rok: 2005/2006

ZADÁNÍ BAKALÁŘSKÉ PRÁCE

(PROJEKTU, UMĚLECKÉHO DÍLA, UMĚLECKÉHO VÝKONU)

Jméno a příjmení:	**Roman KOLAŘÍK**
Studijní program:	**B 3909 Procesní inženýrství**
Studijní obor:	**Technologická zařízení**
Téma práce:	**Modeling of the Film Blowing Process by using Variational Principles**

Zásady pro vypracování:

1. Vypracujte literární studii na dané téma.
2. Proveďte teoretickou analýzu stability procesu vyfukování s využitím variačních principů pro Newtonovskou taveninu.
3. Na základě odvozených stabilitních diagramů ohodnoťte vliv reologie Newtonovských tavenin a procesních podmínek na stabilitu procesu vyfukování.
4. Teoretické závěry ověřte s experimentálními daty provedenými na laboratorní vyfukovací lince.

Rozsah práce:

Rozsah příloh:

Forma zpracování bakalářské práce: **tištěná/elektronická**

Seznam odborné literatury:

1. Kanai, T., Campbell, G.A.: Film Processing, New York (1999).
2. Collyer, A.A., Clegg, D.W.: Rheological Measurement, New York (1998).
3. Agassant, J.F., Avenas, P., Sergent, J.P.H., Carreau, P.J.: Polymer Processing-Principles and Modeling, New York (1991).
4. Zatloukal, M., Vlcek, J.: Modeling of the film blowing process by using variational principles, J. Non-Newtonian Fluid Mech. 123 (2004).
5. Zatloukal, M., Vlcek, J.: Application of variational principles in modeling of the film blowing process for high stalk bubbles, J. Non-Newtonian Fluid Mech. 133 (2006).

Vedoucí bakalářské práce: **doc. Ing. Martin Zatloukal, Ph.D.**
Centrum polymerních materiálů

Datum zadání bakalářské práce: **14. února 2006**

Termín odevzdání bakalářské práce: **13. června 2006**

Ve Zlíně dne 19. ledna 2006

prof. Ing. Josef Šimoník, CSc.
děkan

UNIVERZITA TOMÁŠE BATI VE ZLÍNĚ
Fakulta technologická
L.S.

doc. Ing. Miroslav Maňas, CSc.
ředitel ústavu

ABSTRAKT

Jedním z velmi závažných problémů, který výrazně limituje proces výroby fólií vyfukováním je vznik nestabilního rukávu. I přesto, že v literatuře lze nalézt celou řadu empirických doporučení vedoucích k částečné stabilizaci procesu, není dosud zcela zřejmé, jaký je přímý vztah mezi tokovými charakteristikami polymeru, zpracovatelskými podmínkami a designem zpracovatelského zařízení. Tato skutečnost velmi stěžuje optimalizaci celého procesu. Jednou z možností, jak těmto vztahům blíže porozumět je modelování procesu vyfukování a tvorba stabilitních diagramů. Za tímto účelem se nejčastěji používá Pearson a Petrie model [Pearson, J. R. A., Petrie, C. J. S.: J. Fluid Mech. 40, p. 1, 1970], a to i přes řadu obtíží spojených jak s řešením daného problému (vznik numerických nestabilit, špatná konvergence úlohy) tak s omezenou aplikovatelností. Nedávno však bylo ukázáno, že s využitím variačního počtu lze odvodit model, který výše uvedené nedostatky nemá [Zatloukal, M., Vlcek J.: J. Non-Newtonian Fluid Mech. 123, p. 201-213, 2004; Zatloukal, M., Vlcek, J.: J. Non-Newtonian Fluid Mech. 133, p. 63-72, 2006]. Tento nově navržený model pohlíží na existenci stabilního procesu vyfukování jako na stav, který odpovídá minimálním energetickým nárokům využívající jednoduchých analytických rovnic. Z těchto důvodů byl v této práci použit právě tento model, a to s cílem stanovit stabilitní diagramy hodnotící vliv procesních podmínek, designu vytlačovací hlavy a tokových charakteristik polymeru pro Newtonskou taveninu za předpokladu izotermálních podmínek. Teoretické závěry byly následně porovnány s odpovídajícími experimentálními daty pro lineární a rozvětvený mLLDPE a bylo zjištěno, že predikce modelu jsou v dobré shodě s experimentální realitou pro různé procesní podmínky. Nejdůležitějším závěrem celé práce je zjištění, že vliv pevnosti taveniny je mnohonásobně větší na stabilitu procesu než vliv velikosti Newtonské viskozity což naznačuje, že větvení lineárních materiálů je mnohem efektivnější materiálová modifikace z pohledu růstu stability při vyfukování než prosté zvyšování jejich molekulové hmotnosti. Dalším důležitým závěrem práce je odhalení značného vlivu průměru vyfukovací hlavy a celkové velikosti průtoku na stabilitu procesu což indikuje, že přenositelnost experimentálních stabilitních diagramů z malých laboratorních linek na velké výrobní je velmi omezená.

Klíčová slova: Vyfukování, vytlačování, polymer, modelování polymerních procesů, stabilitní analýza

ABSTRACT

The effect of processing conditions, die design and material characteristics on the stability of the film blowing process for the isothermal Newtonian melt has been investigated theoretically by the recently proposed Zatloukal-Vlcek model [Zatloukal, M., Vlcek, J.: J. Non-Newtonian Fluid Mech. 123, p. 201-213, 2004; Zatloukal, M., Vlcek, J.: J. Non-Newtonian Fluid Mech. 133, p. 63-72, 2006] and the theoretical predictions were compared with the corresponding experimental data. It has been found that the model predictions are in good correspondence with the experimental reality.

Keywords: Blown film, extrusion, polymer, modeling of polymer processing, stability analysis

ACKNOWLEDGEMENT

I would like to express my thanks to all people who contributed to my Bachelor Thesis.

First of all, I am especially thankful and grateful to my supervisor, doc. Ing. Martin Zatloukal, Ph.D. for his valuable advice which helped me create the below-presented results and for his cooperation on the research.

I am also grateful to doc. Ing. Anežka Lengálová, Ph.D. who helped me with English throughout the year and proofread the thesis.

Then I must express my gratitude to doc. RNDr. Petr Ponížil, Ph.D. and Ing. David Sámek, Ph.D. for their, for the time reasons, very important consultation on software.

The support of the project by the Grant Agency of the Academy of Sciences of the Czech Republic (Grant no. KJB2810401) is gratefully acknowledged.

Last but not the least, I would like to extend my gratitude to my family for their support and interest in my work, and I thank my computer for its reliable work all the year round.

I agree that the results of my Bachelor Thesis can be used by my supervisor's decision. I will be mentioned as a co-author in case of any publication.

I declare I worked on this Bachelor Thesis by myself and I have mentioned all the used literature.

Zlín, May 29, 2006 ….…….

Roman Kolařík

TABLE OF CONTENTS

INTRODUCTION

The tubular film blowing process belongs to the oldest polymer processing technologies**.** The basic equipment for the process is a film blowing line. The first commercial line was created in the late 1930´s in the USA. Since then the technology has been developing continuously.

The product of the line is a biaxially-oriented polymeric film of small thickness. This film can be employed for many commercial products used in everyday life. One of the possibilities of the film application is the use in food processing industry, e.g. for carrier bags and food wrapping, another is in the waste industry as refuse bags, waste land fill liners. It can be also used for other purposes such as medical films and etc.

Despite the fact that the film blowing process has a long history and during its lifetime it has been researched both experimentally and theoretically, the clear relationships between the machine design, processing parameters, material and stresses are not completely understood yet. The situation is even more complicated because film blowing process is very sensitive to the onset of the bubble instabilities at particular processing conditions which represents one of the limiting factor for this technology. With the aim to understand these complicated relationships as well as the cause of the bubble instability onset, the modeling of the film blowing process is usually employed. The most popular approach is based on the well known Pearson and Petrie formulation [1]. Even if many useful conclusions about the film blowing process and its stability have been found there exist some difficulties with this approach. Firstly, the use of the Pearson and Petrie formulation leds to the numerical instabilities very well documented in the literature [2], which restrict the solutions for very narrow processing window. Secondly, it has been revealed that the film blowing modeling using this formulation can not predict experimental reality very well especially if the bubble neck becomes to high [3]. With the aim to overcome these noticeable difficulties, recently, novel Zatloukal-Vlcek film blowing model has been derived by the using of the variational principles and successfully tested with the experimental data [4-7]. Moreover, it has been speculated in [5] that this model can predict the bubble instabilities for the processing conditions were the bubble shape does not satisfy the minimum energy requirements i.e. the model solution does not exists in such a case. Thus, the main aim of the present Bachelor Thesis is to use Zatloukal-Vlcek model for the stability contour determination to reveal whether the predicted trends are in quantitative correspondence

with the experimental reality. Specific attention will be paid to the role of the long chain branching on the film blowing stability.

I. THEORETICAL BACKGROUND

1 THE FILM BLOWING PROCESS

The basic equipment for the film blowing process is the film blowing line.

1.1 Description of the film blowing line

The most often used type of the film blowing line is presented in Fig. 1 [1, 8], where the nip rolls are situated on the top of the line.

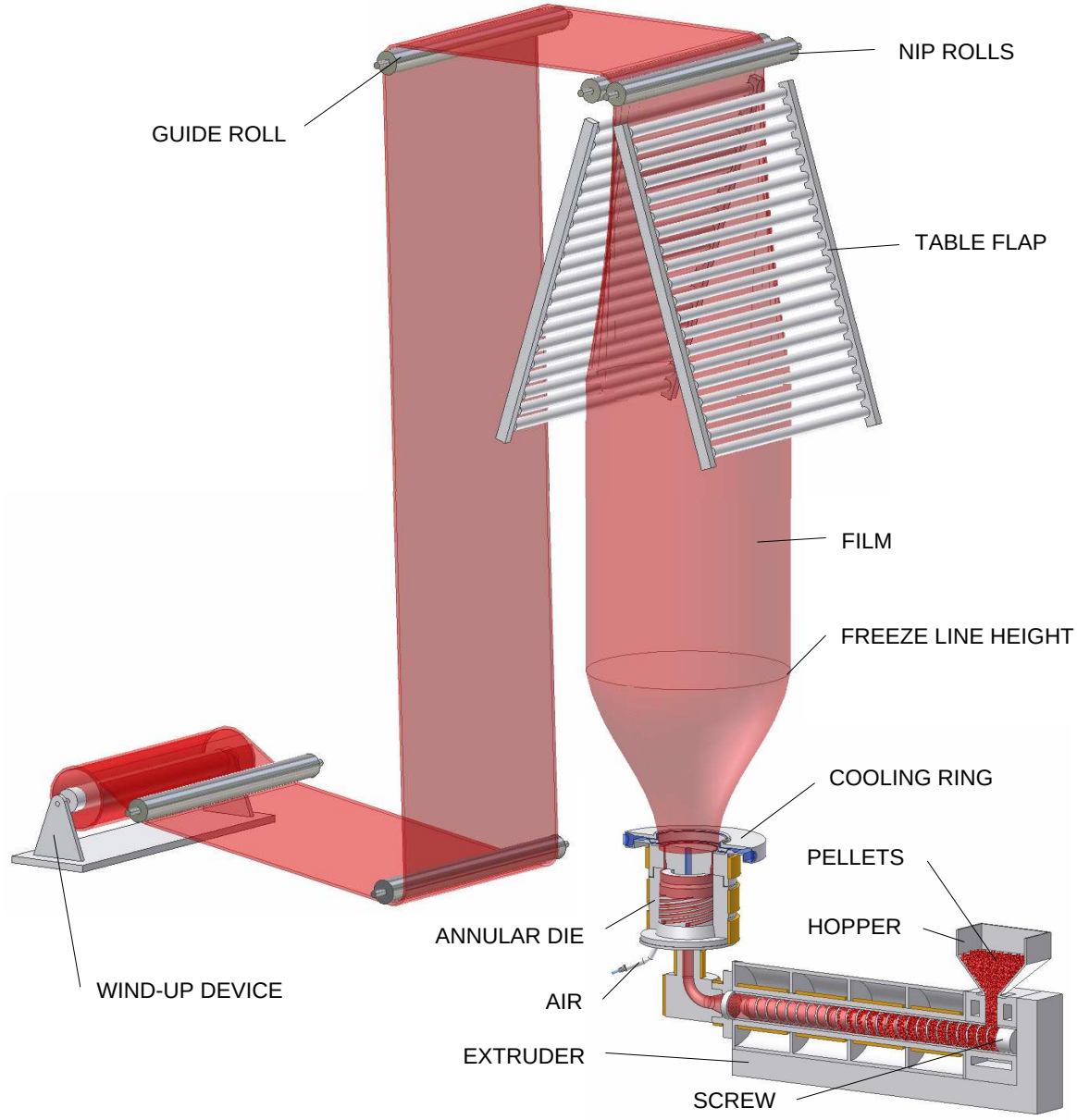

Fig. 1. The film blowing line

In the following part a production of the film blowing is described according to the stated scheme of the film blowing line.

1.2 Description of the process

The process starts in the extruder where polymer pellets are fed to the hopper, inside the extruder they are transported, compressed and melted, and at the end of the barrel the melt is extruded through an annular die. Thence the film is formed to the shape of continuous cylinder that moves in the vertical direction from the annular die. In the area between the annular die and the freeze line height the polymer is in a molten state. The future bubble is created by internal air pressure. With the help of a cooling ring the bubble is cooled to solid film. Air is blown along the bubble surface. This cooling bubble is folded between two table flaps and then two nip rolls close it. Finally, the film is spooled on the cylinder of a wind-up device.

The film blowing process is influenced by two important parameters [9]. One of them is the blow-up ratio:

$$BUR = \frac{R_1}{R_0} \tag{1}$$

which means the ratio of the bubble radius at the freeze line to the bubble radius at the die exit.

Another parameter is the draw-down ratio, which can be written in the following form:

$$DDR = \frac{v_F}{v_D} \tag{2}$$

i.e. the ratio between the film velocity at the freeze line height, L, and at the die exit. The blow-up ratio, *BUR*, together with the draw down ratio, *DDR*, express two directions of the bubble extensions, which is how the film is stretched during the film blowing process. First, axial extension is caused by the nip rolls, whose velocity is an adjustable parameter [5]. It can be one of the possible methods to the film thickness control. Second, circumferential extension is created due to the air pressure inside the bubble. These two directions of the bubble extension produce the final bubble shape.

1.3 Bubble instabilities

Bubble instabilities generate when the film-production speed is higher than a critical speed of the film blowing. More detailed description of instabilities can be found in the works [8, 10-16]. It was observed that the bubble has a lower stability under the following conditions:

- Higher melt temperature (further developed by Han [11, 12]).
- LLDPE bubble without mix of LDPE (details in Obijeski [13]).
- Narrow molecular weight distribution and short chain branching (researched in detail by Kanai and White [14]).

Many different sorts of bubble instabilities can be reached during the film blowing process. The most frequent are presented below in more detail, because they affect the process substantially.

The periodic oscillation of the bubble diameter

The first bubble instability, periodic diameter oscillations, is shown in Fig. 2 [10]; it is also called draw resonance. The instability appears with linear polymers where strain hardening is not present. It occurs in the area of high strain rates. It is very important to know that this instability is not expected to be influenced by the factors which are important for the other ones. There are: first, cooling ring is adjusted untimely, second, formation of the hole on the bubble surface and last, operation of the air pressure on the bubble radius. So, this instability is created first of all by the strain hardening during the high strain rate.

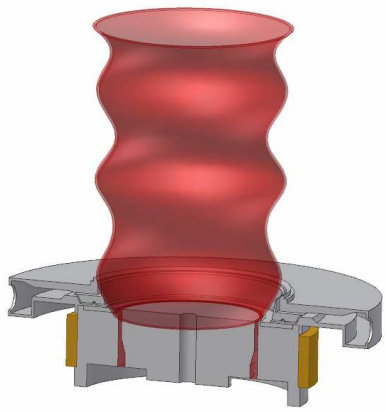

Fig. 2. Draw resonance

Helical instability

Helical instability is created when the air ring is not set-up suitably. Then this instability often appears during the start of the film blowing line. In the scheme presented below (Fig. 3) [10], the right side of the bubble is cooled more than the left side and the helical instability is formed. One possibly way to limit the instability is the modification of the cooling ring, a second possibility is to ensure constant airflow on the bubble surface. However, the first factor affects the bubble stability more than the latter.

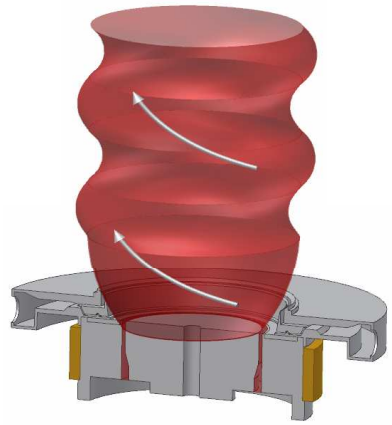

Fig. 3. Helical instability

Instability of the freeze line height (FLH instability)

This bubble instability changes with time, and it is also called periodic oscillation of the freeze line height. It can oscillate in the distance of several centimeters. Although in the presented bubble-point the changed value of the internal bubble pressure and bubble temperature is substantial, the bubble seems to be stable (Fig. 4) [10]. It is because of the almost constant bubble-thickness in the axis direction during the film blowing process. Thus, in this instability only the freeze line height is changed.

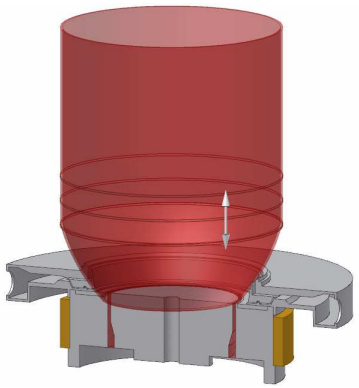

Fig. 4. FLH instability

Heavy-bubble instability

Bubble sag, which is another term for the heavy-bubble instability, is created in the moment when the bubble touches the cooling ring. It is shown in Fig. 5 [10]. Here, the bubble shape in the liquid state changes, which causes worsened bubble surface. This instability is initialized when the bubble touches the cooling ring, i.e. when the force of the cooling air is higher than the tensile strength of the bubble material. After deformation the final bubble has a bigger radius than before.

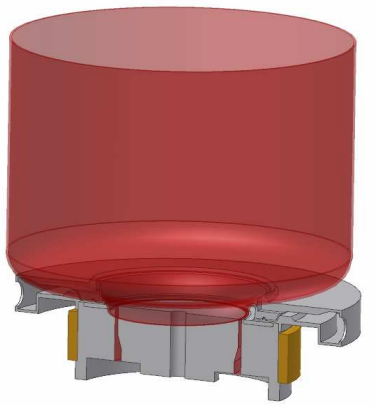

Fig. 5. Bubble sag

Bubble tear

This instability occurs if the tensile stress at the film blowing exceeds the material strength. It means the tensile strength of the film is lower than the take-up force, *F*. Then, in the die exit, the creating bubble is torn in the direction of the acting force, *F* (Fig. 6) [10]. This danger can be reduced by the help of high molecular weight polymers which contain a lot of long chain branching; then the film has stronger structure. It means that this instability is dependent on the polymer structure.

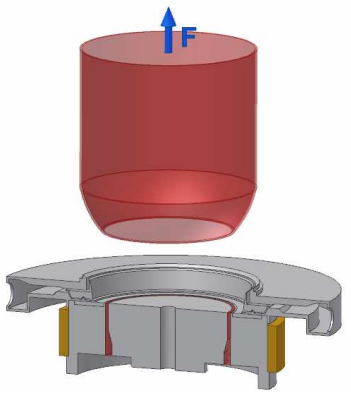

Fig. 6. Bubble tear

Bubble flutter

Bubble flutter instability is caused by the high speed of cooling air. Then the bubble surface is fluttering in the area from the die to the freeze line, as presented in Fig. 7 [10]. When the bubble surface is deformed very intensively, the film has different thicknesses in the molten state. Then it is necessary to limit the exit velocity of the film from the die. Thus, the final speed of the process is limited by the creation of this instability.

Fig. 7. Bubble flutter

The presented bubble instabilities and some more types of instabilities make the prediction of the exit velocity of a particular polymer during the film blowing process very difficult. In agreement with Sweeney [15], bubble stability is influenced by the properties and structure of the polymer, process variables and design of the cooling ring. For the determination of maximum exit velocity, i.e. for the definition of the bubble instability, the design of the cooling ring is very important.

2 MODELING OF THE FILM BLOWING PROCESS

2.1 Review of the current models

In order to model the film blowing process, various model-types can be used for solving the problems in this area. The common models, their descriptions and limitations are presented below in Tab. 1.

Tab. 1. Review of the models dealing with the problems in the film blowing process (adapted from [17])

Author	***Model description***	***Limitations***
Pearson and Petrie [18, 19]	Isothermal Newtonian	Does not incorporate the non-Newtonian flow behaviour of polymer melts
Petrie [20]	Non-isothermal Newtonian and isothermal purely elastic model. Effects of gravity and inertia included	Does not allow for viscoelastic response of materials
Han and Park [21]	Isothermal power law	Does not account for cooling of bubble and viscoelasticity
Wagner [22]	Non-isothermal integral viscoelastic equation with Wagner damping function	Complex, does not accurately estimate stresses at the die exit
Pearson and Gutteridge [23]	Non-isothermal elastic model	Does not allow for the viscoelastic response of materials
Kanai and White [24]	Non-isothermal Newtonian with crystallisation	Does not allow for non-Newtonian behaviour of fluids
Luo and Tanner [2]	Non-isothermal Maxwell model and Leonov models joined together	Solutions highly unstable, the model does not account for non-linear viscoelasticity

Author	*Model description*	*Limitations*
Cain and Denn [25]	Marruci model	Does not account for multiple relaxation time spectrum
Cao and Campbell [26, 27]	Non-isothermal Maxwell model extended above the freeze line with Hookean elastic model	Highly unstable, does not predict creep flow very well
Alaie and Papanastasiou [28]	Non-isothermal integral viscoelastic equation with PSM damping function	Complex, difficult to estimate previous shear history of polymer melt, particularly at the die exit
Liu et al. [29]	Quasi cylindrical bubble combined with non-isothermal power law with crystallization effects constitutive equation	Does not allow for axial curvature of bubble and viscoelastic properties of melt
Sidiropoulos et al. [30, 31]	Modified non-isothermal Newtonian	Does not allow for viscoelastic nature of polymer melt
Zatloukal and Vlcek- (variational principles 1) [5]	Isothermal elastic model (Hookean)	Does not account for the flow behaviour and the bubble movement
Zatloukal and Vlcek- (variational principles 2) [6]	Isothermal Newtonian	Does not incorporate the non-Newtonian flow behaviour of polymer melts
Zatloukal and Vlcek- (variational principles 3) [7]	Non-isothermal non-Newtonian	Membrane approximation. Does not account for flow memory

As one can deduce from the references provided in Tab. 1, the most popular film blowing models are based on the Pearson and Petrie formulation [1, 18, 19]. Moreover, recently proposed variational principle based film blowing formulation [5-7], seems to be breakthrough in the film blowing modeling because it overcomes many of difficulties re-

lated to numerical instabilities and it can also be coupled with the Pearson and Petrie formulation as shown in [6]. Due to that, our attention is paid here to these two formulations only.

2.2 Pearson and Petrie formulation

The standard Pearson and Petrie formulation [1] for the film blowing process includes these assumptions:

- Membrane theory: the bubble is thought to be a thin shell where the film thickness, h, is much smaller than the bubble radius, r, i.e. $h << r$. It can be seen in Fig. 8.
- The bubble movement is time constant and symmetrical around the bubble axis.
- The surface and inertial stresses are neglected due to their low values.

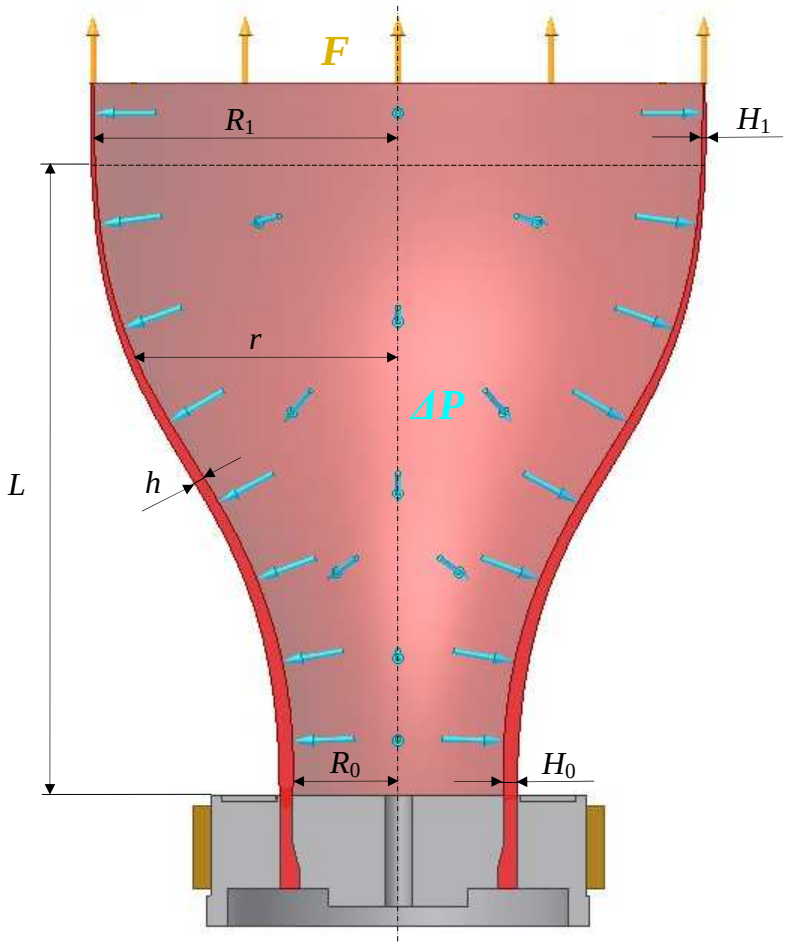

Fig. 8. The film blowing variables

The Pearson and Petrie derivation starts from a local Cartesian coordinate system. The direction x_1 is called the tangential direction, x_2 is the thickness direction, and x_3 is the circumferential direction (Fig. 9).

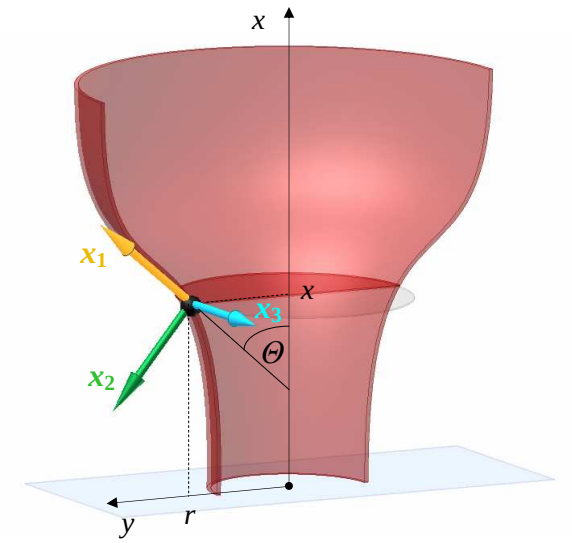

Fig. 9. The Cartesian coordinate system

Derivation of Pearson and Petrie formulation is presented in [1]. The first step of the Pearson and Petrie derivation is the integration of the continuity equation. Then the integration result is obtained in the form

$$Q' = 2\pi r(x)h(x)v(x)\rho(T(x)) \tag{3}$$

As can be seen, every parameter of the equation is a function of x (distance from the die exit). The symbols in the equation have the following meaning: Q' is the mass flow rate, $r(x)$ the bubble radius, $h(x)$ the film thickness, $v(x)$ the film velocity, $T(x)$ the temperature and $\rho(T)$ is the density identified in the study of Spencer and Gilmore [32] as

$$\rho(T) = \frac{1}{\frac{R_g T}{P^* w} + b'} \tag{4}$$

New symbols in the equation are: w - the molecular weight, R_g - the universal gas constant (R_g = 8.314 $J{\cdot}K^{-1}{\cdot}mol^{-1}$), P^* - the cohesion pressure, and b' - the specific volume. For PE, the most common material processed by film blowing, these parameters are given in the work of Hellwege et al. [33]: $w = 28{\cdot}10^{-3}$ $kg{\cdot}mol^{-1}$, $b' = 8.75{\cdot}10^{-4}$ $m^{3}{\cdot}kg^{-1}$ and $P^* = 3.18{\cdot}10^{8}$ Pa. Thus, the previous equation is obtained in form:

$$\rho(T(x)) = \frac{10^3}{0.934 \cdot 10^{-3} T(x) + 0.875} \tag{5}$$

If the momentum equation and membrane theory are taken together, the internal bubble pressure, ΔP, can be expressed in the following form, as shown in [1]:

$$\Delta P = \frac{h\sigma_{11}}{R_m} + \frac{h\sigma_{33}}{R_t} \tag{6}$$

Parameters σ_{11} and R_m are the tangential directions of the stress and curvature radius, respectively. Further, parameters σ_{33} and R_t mean the circumferential directions of the stress and curvature radius, respectively. The presented curvature radii have a form

$$R_t = \frac{r}{\cos(\theta)} \tag{7}$$

$$R_m = \frac{-1}{\frac{d^2 r}{dx^2}\cos^3(\theta)} \tag{8}$$

Term $\cos(\theta)$ in Eqs. (7) and (8) is calculated as:

$$\cos(\theta) = \frac{1}{\sqrt{1 + \left(\frac{dr}{dx}\right)^2}} \tag{9}$$

The force balance in the perpendicular direction has the form

$$2\pi r h \sigma_{11} \cos(\theta) = F - \pi \Delta P \left(r_f{}^2 - r^2\right) - G + H \tag{10}$$

where r_f is the bubble radius at the freeze line height, F means the take-up force, G stands for the gravity, and H is the force created by the air flow. By using Fisher's assumption [34], forces G and H have the same value, i.e. the presented equation is not influenced by these forces. Then Eq. (10) can be reduced to

$$2\pi r h \sigma_{11} \cos(\theta) = F - \pi \Delta P \left(r_f{}^2 - r^2\right) \tag{11}$$

From this Equation, stress σ_{11} can be expressed as

$$\sigma_{11}(x) = \frac{F - \pi \Delta P \left(r_f{}^2 - r(x)^2\right)}{2\pi r(x) h(x) \cos(\theta(x))} \tag{12}$$

Stress $\sigma_{11}(x)$ is a distance function from the annular die, *x*, as well as a function of parameters *r*(*x*), *h*(*x*) and $\cos(\theta(x))$. The equation for stress $\sigma_{11}(x)$ has a specific form in the area of the freeze line height, *L*. If the line slope $\left(\frac{dr}{dx}\right)$ is equal to zero, the tangential stress $\sigma_{11}(L)$ at the freeze line height can be rewritten into the following form:

$$\sigma_{11}(L) = \frac{F}{2\pi R_1 H_1} \tag{13}$$

where the bubble radius at the freeze line height is $R_1 = R_0 BUR$, and H_1 is the bubble thickness at the same place.

With the help of Eq. (6), the stress in the circumferential direction is stated in the form

$$\sigma_{33}(x) = \frac{R_t(x)}{h(x)}\left(\Delta P - \frac{h(x)}{R_m(x)}\sigma_{11}(x)\right) \tag{14}$$

This stress at the freeze line height then will be

$$\sigma_{33}(L) = \frac{R_1}{H_1}\Delta P \tag{15}$$

Now, stresses σ_{11} and σ_{33} are known for both directions, i.e. for the tangential and circumferential directions, respectively. Thus these stresses can be calculated for various distances from the die exit to the freeze line height, i.e. for *x*.

Applying the above-mentioned assumption (h << r), it is possible to expect $|\sigma_{22}| << |\sigma_{33}|$ and $|\sigma_{22}| << |\sigma_{11}|$. It means that $\sigma_{22} = 0$ and from the calculation $\sigma = -pI + \tau$ the following equation expresses the proportion between the total stresses, σ, and the extra stresses, τ (*p* – pressure, *I* – unit tensor):

$$\begin{aligned} \sigma_{11} &= \tau_{11} - \tau_{22} \\ \sigma_{22} &= 0 \\ \sigma_{33} &= \tau_{33} - \tau_{22} \end{aligned} \tag{16}$$

In the solution of the equations used in the Pearson and Petrie formulation, the following two problems arise:

- Numerical instabilities [2, 4, 5]
- Bubble-shape description [3-5]

Let us have a closer look at them.

Numerical instabilities

These types of instabilities are usually caused by inability of the numerical scheme to converge for the certain polymer rheology, processing and boundary conditions or by existence of the multiple solutions. Moreover, the solution is very sensitive to the initial bubble angle at the die exit as well as melt history related to the die flow. Due to that, the solution available for only a small area of the operating conditions. This is discussed in more detail by work of Luo and Tanner [2].

Problems with the bubble-shape description

These problems are connected with high stalk bubbles, i.e. bubbles with a long neck. Here, the bubble shape with the original elongated neck is not described exactly - the predicted values start earlier than the elongated neck of the bubble in reality.

The presented problems of Pearson and Petrie model should be eliminated by the use of the Zatloukal and Vlcek formulation derived by the variational principles, which are described in the following part in more details.

2.3 Zatloukal and Vlcek formulation

Zatloukal and Vlcek formulation is based on the idea that the film blowing process satisfies minimum energy requirements and variational principles can be used to derive a model which describes the bubble creation. In more detail, it is well-known that bubble shape changes during the film blowing process. It happens due to the internal load, p, and the take-up force, F. The bubble can be understood as a static flexible membrane. It means that the thickness is a neglected parameter because the membrane is a very thin layer. It can be found in two shapes. First, bubble shape before deformation (Fig. 10) [4, 5]; here

the line element of the membrane is *dx*. Second, bubble shape after deformation (Fig. 11) [4, 5], where the bubble shape is given by the following equation [4, 5]:

$$\sqrt{1+(y')^2}\,dx \approx \left[1+\frac{1}{2}(y')^2\right]dx \qquad (17)$$

This is valid in the area from the annular die radius, R_0, to the freeze line height, L. It has been shown in [5] that if the constant bubble compliance is assumed, one can derive the analytical equation for the bubble shape satisfying the minimum-energy requirements by using variational principles.

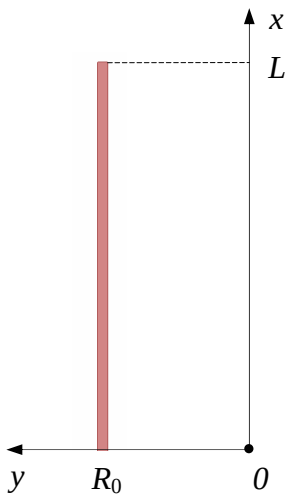

Fig. 10. Membrane before deformation

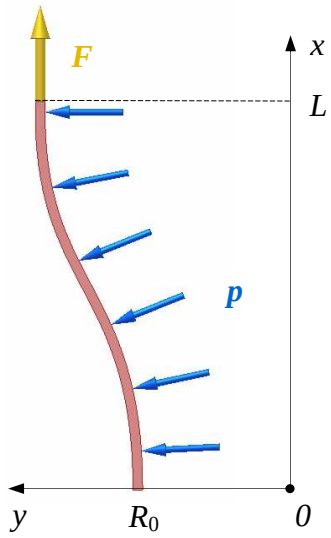

Fig. 11. Membrane after deformation

In more detail, equations for both types of the bubble shapes can be derived: without and with a neck.

Bubble without neck

For the bubble shape description the following four parameters have to be known. First, it is the freeze line height, L, second is parameter pJ, which is compound of both the membrane compliance, J, together with the internal load, p. The next is the blow up ratio, BUR, and the final parameter is the die radius, R_0.

It has been shown in [5] that any equation for the bubble that satisfies the following differential equation also satisfies the minimum-energy requirements:

$$Fy'' - \lambda_1 2\pi y + p = 0 \tag{18}$$

Here, F is the take-up force, λ_1 stands for the Lagrange multiplier, p means the internal load, and y is the equation of the bubble shape. It is not difficult to show (see [4, 5] for more detail) that the Eq. (19) satisfies the Eq. (18) and thus can be considered as the simplest expression for the bubble shape

$$y = (R_0 - pJ)\cos\left(\frac{x\varphi}{L}\right) - \alpha'(pJ - BURR_0)\sin\left(\frac{x\varphi}{L}\right) + pJ \tag{19}$$

In this equation the parameters are:

- Parameter x is a positive number from *0* to the freeze line height, L
- Parameter α' is defined as:

$$\alpha' = \sqrt{\frac{2pJ - R_0 - BURR_0}{pJ - BURR_0}\left|\frac{R_0(BUR-1)}{pJ - BURR_0}\right|} \tag{20}$$

- Parameter φ is stated in Tab. 2, where A is given by the following equation:

$$A = \frac{pJ - R_0}{pJ - BURR_0} \tag{21}$$

Tab. 2. Parameters A and φ for different bubble shapes (y). Parameter A is equal to A´´ and parameter φ´´ is same as φ.

Equation	***A***	***φ***	***y***
1.	1	0	R_0
2.	0<A<1	$arctg\left(\frac{\sqrt{1-A^2}}{A}\right)$	The form of Eq. (19)
3.	0	π/2	$R_0\left\{1-\sin\left(\frac{x\pi}{2L}\right)(1-BUR)\right\}$
4.	-1<A<0	$\pi + arctg\left(\frac{\sqrt{1-A^2}}{A}\right)$	The form of Eq. (19)
5.	-1	π	$\frac{R_0}{2}\left\{1+\cos\left(\frac{x\pi}{L}\right)(1-BUR)+BUR\right\}$

Finally, the equation for the take-up force can be obtained in the following form:

$$F = -\frac{L^2}{J\varphi^2} \tag{22}$$

The introduced Eqs. (13), (15), (19-22) and Tab. 2 will be used in the experimental part of the Bachelor Thesis, together with the below presented Eq. (32).

Bubble with the neck height

This type of the bubble consists of two sections (Fig. 12) [5]. The first is influenced by the uniaxial stretching up to the distance L_1. The radius of the bubble is changed from R_0 to R_0BUR. Thus the bubble can be described by equation:

$$y_1 = (R_0 - pJ)\cos\left(\frac{x\varphi''}{L_1}\right) + \alpha''(pJ - BUR_0R_0)\sin\left(\frac{x\varphi''}{L_1}\right) + pJ \tag{23}$$

This equation is generated from several parameters:

- Parameter φ'' is identified with the aid of the Tab. 2 according to the value A'', where BUR_0 is supplying BUR in Eq. (20) and their dependence is:

$$BUR_0 = \frac{BURR_0}{2pJ - R_0} \tag{24}$$

  It means that parameter A'' can be written in the form:

$$A'' = \frac{pJ - R_0}{pJ - BUR_0R_0} \tag{25}$$

- Parameter α'' has the same substitution as parameter A''. Then it is defined as

$$\alpha'' = \sqrt{\frac{2pJ - R_0 - BUR_0R_0}{pJ - BUR_0R_0}\left|\frac{R_0(BUR_0 - 1)}{pJ - BUR_0R_0}\right|} \tag{26}$$

- The neck height L_1 is identified by equation

$$L_1 = \frac{\varphi''\left(L\varphi'' - \pi\sqrt{-\xi}\right)}{\varphi''^2 - \pi^2} \tag{27}$$

where ξ is

$$\xi = pJR_0\left(2BUR_0 - 1 - BUR\right)\left(\pi^2 - \varphi''^2\right) - L^2 \tag{28}$$

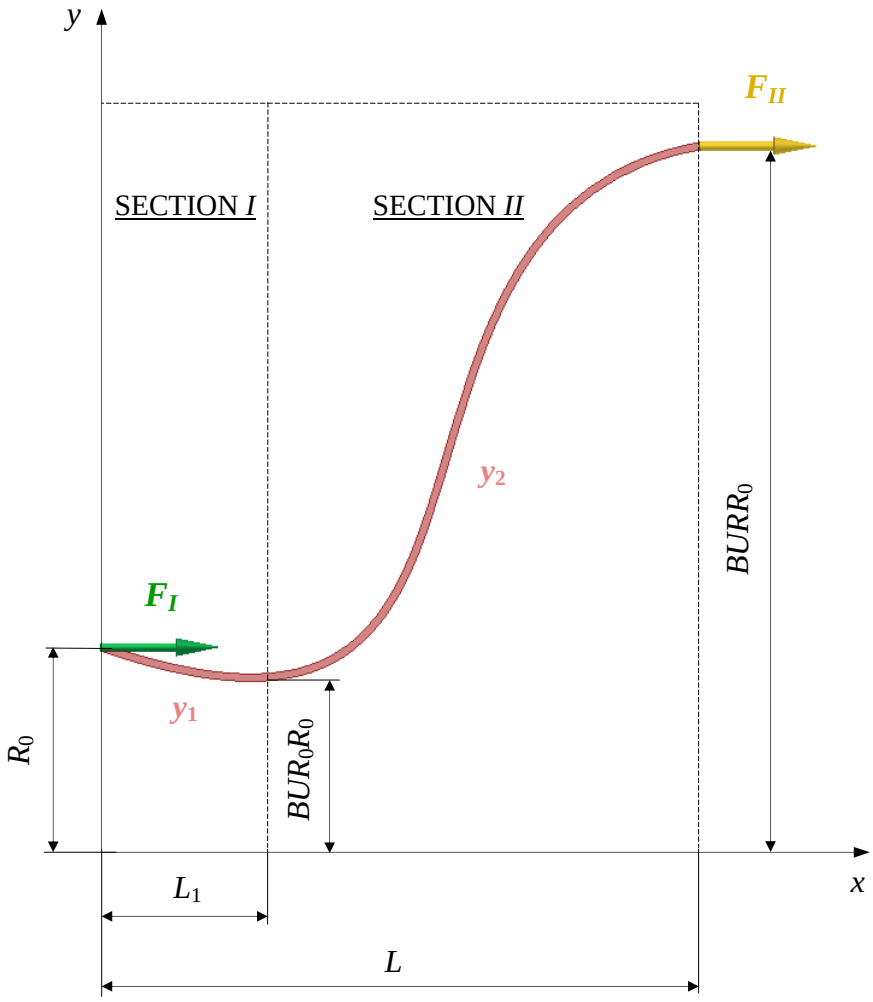

Fig. 12. Bubble with neck height – acting forces

Tensile force F_I, acting at the die exit in the direction from the annular die, is expressed as

$$F_I = -\frac{L_1^2}{\varphi''^2 J} \tag{29}$$

Different conditions can be identified in the second section of the neck (the area $L - L_1$). Here the material is deformed by biaxial stretching. At the freeze line height, L, the radius of the bubble is equal to R_0BUR. This bubble section is described as:

$$y_2 = BUR_0\left\{pJ + \cos\left[\frac{(x - L_1)\pi}{L - L_1}\right](R_0 - pJ)\right\} \tag{30}$$

The tensile force acting at the freeze line height can be written in the following form:

$$F_{II} = -\frac{(L - L_1)^2}{\pi^2 J} \tag{31}$$

Internal bubble pressure

The internal bubble pressure can be expressed in this form [5]:

$$\Delta p = \frac{pL}{2\pi\int_0^L y\sqrt{1 + (y')^2}\,dx} \tag{32}$$

Here, *pL* represents the force acting at the bubble thickness in the perpendicular direction, and expression $2\pi\int_0^L y\sqrt{1 + (y')^2}\,dx$ defines the surface of the bubble. The internal bubble pressure is calculated for a cylinder whose surface area is the same as in the case of the existing bubble.

Comparison of the bubble with and without the neck height

Bubbles without the neck are limited by two parameters pJ, i.e. from pJ_1 to pJ_2. Then the bubbles with the neck height are offered in the area of pJ_2 to pJ_3, as can be seen in Fig. 13. The bubble shape curvatures are influenced by the internal load, *p*, and the membrane compliance, *J*. If one of the parameters is high, the bubble shape curvature is also high, and vice versa.

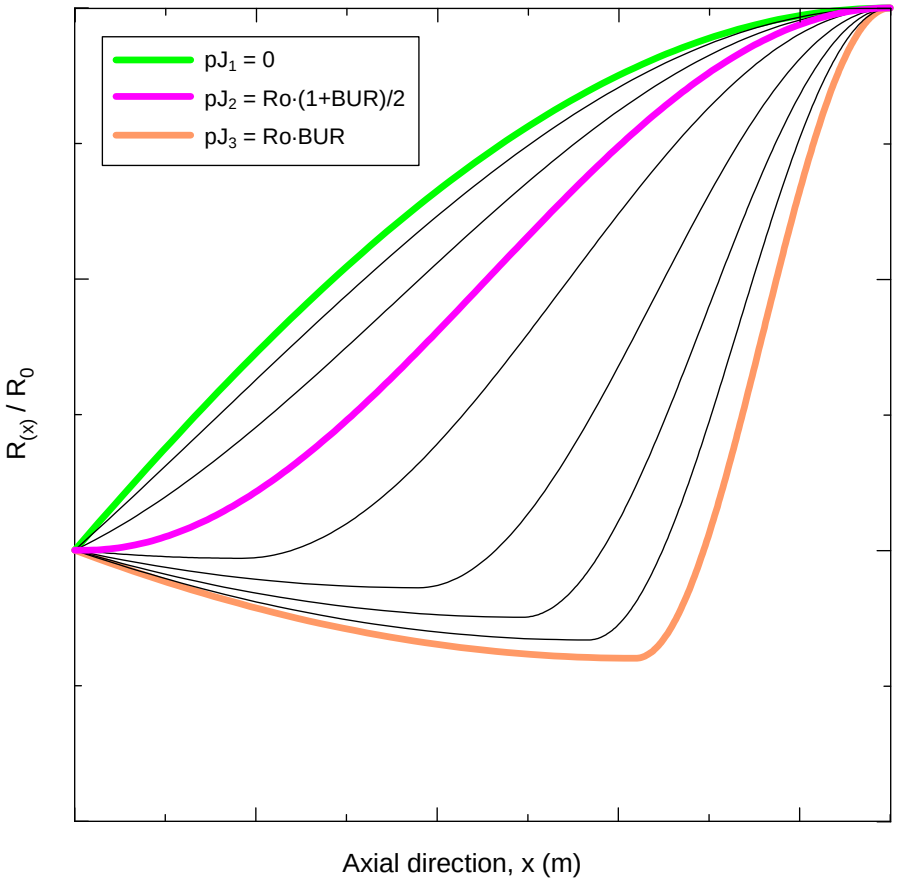

Fig. 13. Bubble shapes with different values of pJ. Parameters BUR, R_0 and L are constant [5].

If the above described Zatloukal-Vlcek formulation is combined with the continuity, constitutive and energy equations, one can derive additional mathematical expressions for the compliance *J* and freeze line height *L*. In such case, the film blowing model becomes fully predictive. Moreover, it has been suggested in [5] that critical points predicted by the model can be related to the bubble instabilities widely described in the literature. This might be explained by the fact that Zatloukal-Vlcek formulation allows to predict bubbles which are acceptable from the minimum energy point of view.

3 AIMS OF THE WORK

The main aim of this work is to determine the stability contours (relative final film thickness vs. *BUR*) derived from the Zatloukal-Vlcek formulation for an isothermal conditions and Newtonian fluids. In more detail, the effect of material properties (Newtonian viscosity, rupture stress of the melt), process conditions (freeze line height, volume flow rate, internal load and internal bubble pressure) and die design (die radius) on the bubble stability will be investigated. The predicted stability contours and trends will be compared and discussed with the real experimental data. Specific attention will be paid to the effect of the long chain branching on the stability of the film blowing process.

II. EXPERIMENTAL

4 MATERIALS

In this work, two metallocene based LLDPE were used for the experiments on the film blowing line. In more detail, both mLLDPEs are chemically identical and the only difference is that the first mLLDPE is linear whereas the second one is branched. It should be pointed out that no additional information about these two materials are mentioned in this work because the institution providing these materials is wishing to keep this information as confidential.

5 FILM BLOWING EXPERIMENT

The experimental work on the film blowing line has been done in cooperation with the University of Bradford. The parameters of the film blowing process (internal bubble pressure, Δp, volumetric flow rate, Q, die gap, H_0, bubble radius at the die exit, R_0, freeze line height, L) were obtained from measurements on the film blowing line depicted in Figs. 15a-15b, which is composed from a Betol BC 38 mm single screw extruder equipped by Davis Standard model DSBMT barrier screw (Figs. 15d-15e) and spiral mandrel die having six feeding channels with annulus diameter and the gap equal to 74 mm and 1.34 mm, respectively, as visible in Fig. 15c. More details about the experimental set-up are provided in [16]

The basic point of the experimental work was the determination of the processing window for linear and branched mLLDPE. The main experimental results are depicted in Fig. 14 where the experimentally determined stability diagrams (relative film thickness vs. *BUR*) for linear and branched mLLDPE are provided. The areas above and bellow the blue/pink lines represent stable and unstable film blowing conditions, respectively. It is nicely visible that the branched mLLDPE is much more stable compared to linear mLLDPE material. In the other words, branched mLLDPE can be used to produce thinner film at a higher *BUR* in contrary to the linear mLLDPE.

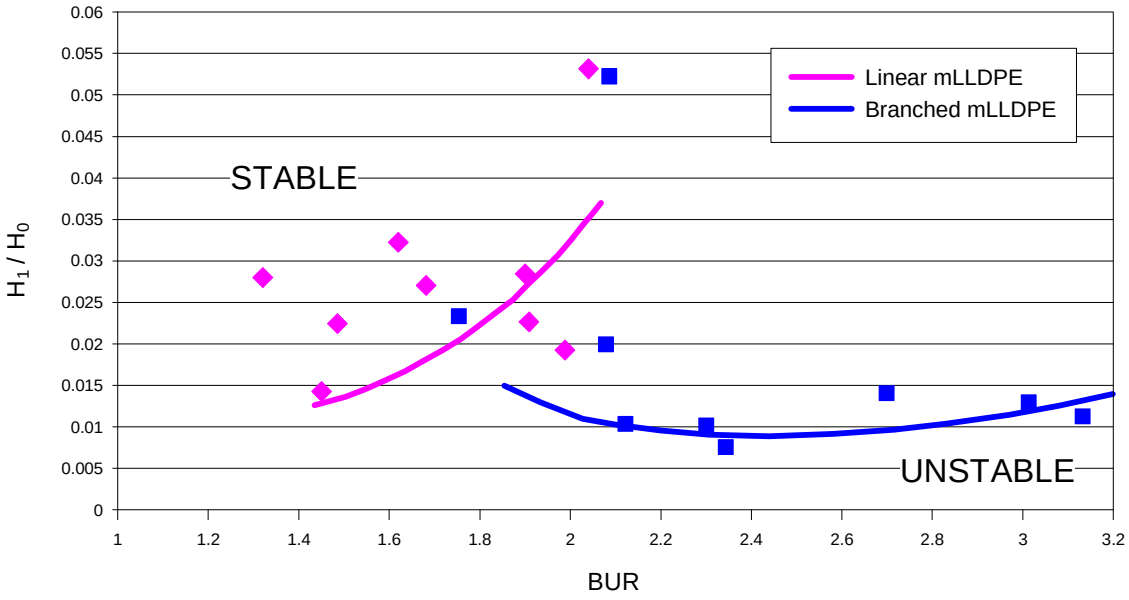

Fig. 14. The experimentally determined stability contours for both, linear and branched metallocene LLDPE bubbles (FLH 180 mm and temperature 190°C).

15a)

15c)

15b)

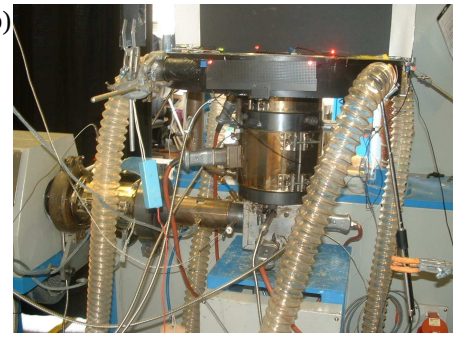

15d)

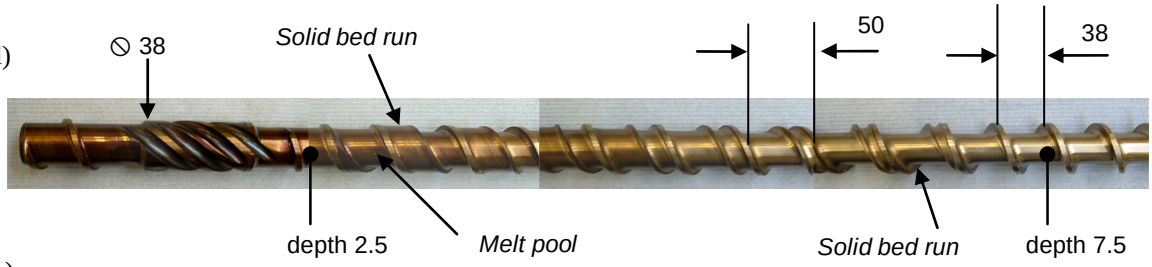

15e)

Fig. 15. Film blowing experimental set-up at the University of Bradford, UK. 15a) General view of the experimental film blowing line; 15b) Closer view of the film blowing die; 15c) Used spiral mandrel; 15d) DSBMT barrier screw with a 24:1 L/D and barrier flighted with spiral Maddox mixer; 15e) Detail picture of the Maddox mixer (egan type).

RESULTS AND DISCUSSION

At the beginning of the research, it is necessary to check, whether Zatloukal-Vlcek film blowing model has capability to describe the experimentally observed bubble shapes for linear as well as branched mLLDPEs produced under different processing conditions. In Fig. 16 it is clearly demonstrated that the model has extremely high fitting capability to describe all measured bubble shape observed on the Bradford film blowing line.

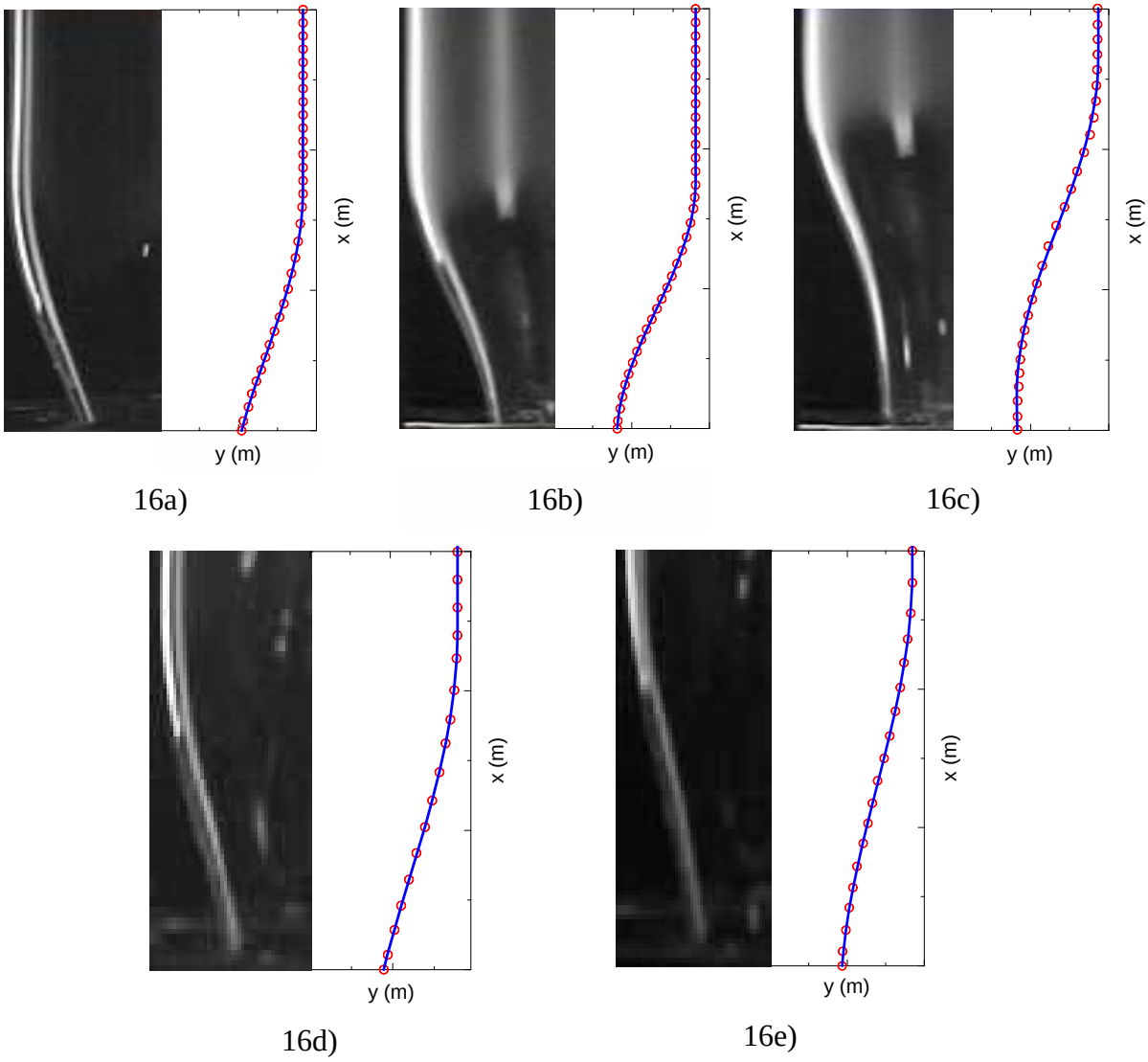

Fig. 16. Comparison between experimental data (∘) and the Zatloukal-Vlcek model prediction (—) for linear as well as branched mLLDPEs. Processing conditions for each bubble are summarized in Tab. 3. 16a) Bubble 1: Highly branched mLLDPE; 16b) Bubble 2: Linear mLLDPE; 16c) Bubble 3: Linear mLLDPE; 16d) Bubble 4: Slightly branched mLLDPE; 16e) Bubble 5: Slightly branched mLLDPE.

The processing conditions for all bubbles depicted in Fig. 16 are summarized in Tab. 3. Note that for all cases, the freeze line height is virtually the same, i.e. equal to 0.18 m. The bubbles with no neck (1-2, 4-5) were described by the Eq. (19) whereas the description of the bubble with neck height (3), has been done by Eqs. (23) and (30). The corresponding compliances summarized in the Tab. 4 were determined from the measured internal bubble pressure for the individual processing conditions summarized in Tab. 3.

Tab. 3. The table of the experimental conditions for the constant bubble-parameters: $R_0 = 0.037$ m, $H_0 = 0.00134$ m, $L = 0.18$ m, $\rho = 750$ kg·m^{-3}

Bubble	***mLLDPE***	***Q*** ***(m^3·s^{-1})***	***H_1*** ***(m)***	***v_F*** ***(m·s^{-1})***	***Δp*** ***(Pa)***	***BUR*** ***(-)***
1	Highly branched	$5.133 \cdot 10^{-6}$	$31.00 \cdot 10^{-6}$	0.1500	95.157	1.958
2	Linear	$4.344 \cdot 10^{-6}$	$30.00 \cdot 10^{-6}$	0.2167	155.979	1.967
3	Linear	$4.344 \cdot 10^{-6}$	$26.00 \cdot 10^{-6}$	0.2167	142.637	2.046
4	Slightly branched	$2.985 \cdot 10^{-6}$	$26.50 \cdot 10^{-6}$	0.2167	147.150	2.142
5	Slightly branched	$2.626 \cdot 10^{-6}$	$31.25 \cdot 10^{-6}$	0.1830	161.865	1.810

Tab. 4. Zatloukal-Vlcek model fit parameters for experiments provided in Tab. 3

Bubble	***mLLDPE***	***L*** ***(m)***	***pJ/R_0*** ***(-)***	***J*** ***(Pa^{-1})***	***F*** ***(N)***	***BUR*** ***(-)***
1	Highly branched	0.18560	1.298229	0.001501	4.47009	1.761
2	Linear	0.18000	1.604832	0.000988	3.53031	2.214
3	Linear	0.18600	1.608108	0.001382	1.95209	2.210
4	Slightly branched	0.18305	1.359514	0.000917	7.78050	2.000
5	Slightly branched	0.18206	1.470525	0.000952	4.22161	1.959

Closer inspection of the Tabs. 3 and 4 (especially the comparable processing conditions where the final film thickness takes the same value, i.e. Bubble 1, 2 and 5) reveals that the model predicts increase of the take-up force with the increasing level of the long chain branching, which is expected trend because long chain branching increases the extensional strain hardening and thus resistance to the extensional flow. This also supports the physic behind the Zatloukal-Vlcek model.

Based on the above analysis, it can be said that the used model has very good capability to describe the experimental data for the film blowing experiments for linear as well as branched mLLDPEs. Therefore, the model seems to be suitable for bubble stability investigation.

For the stability contour determination it is assumed that the bubble is unstable if it does not satisfy the minimum energy requirement, i.e. if A<-1 (it is called here as 'model stability contour') or if the tensile stresses in the machine/circumference directions exceed the material bubble strength (it is called here as 'machine' or 'circumference stress stability contour'). In this work, the stability contours stand for curves in the reduced final film thickness vs. *BUR* graph determining stable processing window. Typical stability contour for the particular material and processing conditions predicted by the model is depicted in Fig. 17. In the section bellow, it is shown, in what way these stability contours are calculation for the following assumptions:

1. the film blowing process is isothermal,
2. the polymer material is Newtonian,
3. the velocity profiles is linear between the die and the freezline,
4. the bubble with the neck height is not considered.

Model stability contour

The limit determines the maximum film thickness in a definite range of parameter *BUR*. It means that the goal of the calculation is the film thickness, H_1, at the freeze line height, L. The basic step in the calculation is creation of an equation for the membrane compliance in the case of the bubble without neck. This equation is based on the balance of forces F_I and $F_{II,N}$, which are the acting forces at the die and freeze line height, respectively. Force F_I is given in a positive value by Eq. (22) from the variational principle. The

other force, $F_{II,N}$ results from the connection of the equations of continuity and Newton model, which are given below [6]:

$$Q = 2\pi r(x)h(x)v(x) \tag{33}$$

$$\tau = 2\eta_0 D \tag{34}$$

where parameter Q is the volumetric flow rate, τ means the extra stress, η_0 stands for the Newtonian viscosity and D represents the deformation rate tensor. Then, force $F_{II,N}$ can be expressed in the following form

$$F_{II,N} = 2\eta_0 \dot{\varepsilon}_1 \frac{Q}{v_F} \tag{35}$$

If Eqs. (22) and (35) are taken to the balance, then the equation of the membrane compliance can be written as

$$J = \frac{L^2 v_F}{2\eta_0 \dot{\varepsilon}_1 \varphi^2 Q} \tag{36}$$

This parameter can be also expressed for a boundary condition of the variational principle, which is defined by parameter $A = -1$ (Tab. 2) and Eq. (21). Thus, the equation is

$$J = \frac{R_0}{2p}(1 + BUR) \tag{37}$$

After the connection of Eqs. (36) and (37), it is necessary add an equation of the extensional rate for a linear process in the form

$$\dot{\varepsilon}_1 = \frac{v_F - v_D}{L} \tag{38}$$

where the velocities v_F and v_D represent the film velocity at the freeze line height and die, respectively. The velocities are determined from Eq. (33), where the terms for die gap $h(x) = H_0$ and bubble radius at the die exit $r(x) = R_0$ are used for the calculation of the velocity at the die. For the determination of the velocity at the freeze line height, the terms in question are given in the forms: $r(x) = R_1 = R_0 BUR$ and $h(x) = H_1$.

If Eqs. (36-38) are joined, then the film thickness at the freeze line height has the following form

$$H_1 = \frac{R_0(1+BUR)Q\eta_0\pi^2 - pL^3}{2\pi^3 R_0^2 \eta_0 v_D BUR(1+BUR)} \tag{39}$$

Machine stress stability contour

During the film blowing process the film is taken up by the nip rolls, where the maximum take up velocity/force is given according to the film strength in the axis direction. This criterion is expressed by the film thickness at the freeze line height, H_1, in the fixed range of parameter *BUR*. The calculation is based on the Newton model (34). Here, Eq. (38) is used, too. Then, the film thickness is calculated as

$$H_1 = \frac{Q\eta_0}{\pi R_0 BUR(\sigma_{11}L + 2\eta_0 v_D)} \tag{40}$$

Circumference stability contour

The film is expanded by air pressure, which also determines the film thickness. The value of air pressure must not get above the value of the film strength in circumferential direction. It means, again, that the goal of the calculation is to find the film thickness at the freeze line height, H_1, in a specific area of *BUR* parameter. This thickness is given by Eq. (15) and is defined as

$$H_1 = \frac{R_0 BUR}{\sigma_{33}}\Delta p \tag{41}$$

where the internal bubble pressure is given by Eq. (32).

Here, the presented equations do not contain any parameter of viscosity. For this reason Eq. (21) is necessary to be rewritten as the membrane compliance:

$$J = \frac{R_0(ABUR-1)}{p(A-1)} \tag{42}$$

Then, using Eqs. (36), (38) and (42) the Newtonian viscosity can be obtained in the following form

$$\eta_0 = \frac{pL^3 v_F (A-1)}{2Q\varphi^2 R_0 (v_F - v_D)(ABUR-1)} \tag{43}$$

Effect of Newtonian viscosity on the film blowing stability

Predicted effect of the Newtonian viscosity on the film blowing stability is depicted in Figs. 18-20. It is clearly visible that an increase in the Newtonian viscosity leads to the increase of the film blowing processing window. In more detail, the Fig. 18 reveals that an increase in the Newtonian viscosity (i.e. Mw) of the melt increases the capability to achieve much higher final film thickness for certain *BUR* which is very desirable for heavy-duty bags production. On the other hand, the model predicts that an increase in the Newtonian viscosity increases the stretch ability of the melt, i.e. one can produce lower final film thickness compared to the case where the material has lower Newtonian viscosity as visible in Figs. 19-20.

Effect of melt strength on the film blowing stability

Predicted effect of the melt strength on the film blowing stability is visualized in Figs. 21-22. It is nicely visible that an increase in the melts strength (even if it is very small) significantly increases the capability to produce very thin films. As visible in Fig. 19, such dramatic increase of the stretch ability can not to by achieved through an increase in Newtonian viscosity (even if the viscosity increase is very high in this case). On the other hand, the model predicts that an increase in the melt strength does not increase the capability to produce thick films as clear from the Fig. 21. It should also be noted that significant stabilization of the film blowing process by introducing the long chain branching (see Fig. 14) can be explained by increased melt strength as showed theoretically in this chapter. This will be discussed in more detail in the below mentioned chapter.

Effect of freeze line height on the film blowing stability

Even if it is assumed in this work that the film blowing process is view as the isothermal, it is possible partially investigate the effect of the cooling conditions on the film blowing process stability by investigating how the increase of the freeze line height (i.e. decrease in the heat transfer coefficients) influences the process stability. Figs. 23-25 clearly proves that the decrease of the freeze line height (by increasing the heat transfer coefficients for example) significantly improves the bubble stability. This conclusion is in very good agreement with the work of Han [11, 12] who has shown that an increase in the

melt temperature (which is equivalent to the heat transfer coefficient decrease which causes that the freeze line height increases) leads to the more unstable bubble.

Effect of die radius and volume flow rate on the film blowing stability

The predicted effect of the die radius and volume flow rate on the film blowing stability is depicted in Figs. 26-31. It is again clearly visible that an increase in the die radius and volume flow rate significantly increases the stability of the process. This practically means that the stability of the process is much higher on the big production lines compared to the small laboratory equipments having usually significantly smaller die radius as well as lower production rate (i.e. volume flow rate) compared to big lines. This suggests that the scale-up procedure based on the small laboratory film blowing lines may not be reliable from the film blowing stability point of view.

Effect of internal load on the film blowing stability

The Figs. 32-34 show that decrease in the internal load leads to more bubble stability process. On the other hand, one should keep in mind that the reduction of the internal load decreases the level biaxial film orientation which may leads to very poor properties of the final film.

Experimental stability contours vs. predicted ones

In this part, we have tried to follow the experimental data from the Bradford film blowing line depicted in Fig. 14 numerically to see, whether the Newtonian, isothermal Zatloukal-Vlcek model can predict the trends properly. The well designed rheological experimental characterization of the linear and branched mLLDPEs performed by Musil in his Bachelor Thesis [35] reveals that an increase in the long chain branching just very slightly increases the Newtonian viscosity whereas the melt strength increases significantly. Therefore, the Newtonian viscosity of the melt has been kept as a constant for both linear and slightly branched mLLDPE and the melt strength for both materials were varied to find out the agreement with the experimentally determined stability contours depicted in Fig. 14. The comparison between the measured and fitted stability contours are depicted in

Fig. 35. It is clearly visible that the agreement between theoretical and experimental data is very good. Moreover, the melts strength, which has been taken as the free adjustable parameter in this case, is higher for more stable branched mLLDPE and vice versa. This again supports the physical background behind the model and confirms the trends in the measured melt strengths for both materials in the Musil [35].

At the end of this section, it should be mentioned that in Figs. 18-34, the level of the internal bubble pressure in *Pa* appears directly along corresponding stability contour.

CONCLUSION REMARKS

1. It has been shown that the Zatloukal-Vlcek model has very good capability to describe the bubble formation of the linear as well as branched mLLDPEs under different processing conditions.

2. It has been theoretically revealed that an increase in the Newtonian viscosity, melt strength, die radius and volume flow rate increases the stability of the film blowing process. On the other hand, it has been revealed that increase in the freeze line height and internal load decreases the process stability. In more detail, it has been revealed that the melt strength has much higher influence on the bubble stability than Newtonian viscosity. This suggests that introduction of the long chain branching into linear polymer is much effective for bubble stabilization than only molecular weight increase.

3. Based on the theoretical stability analysis, it has been suggested that the commonly used scale-up procedure based on the small laboratory film blowing experiments may not be reliable from the film blowing stability point of view because it seems that the die radius and volume flow rate have significant influence on the process stability.

4. It has been revealed that the long chain branching significantly improves the stability of the film blowing process due to increasing melt strength, which has been proved from both, experimental and theoretical investigations.

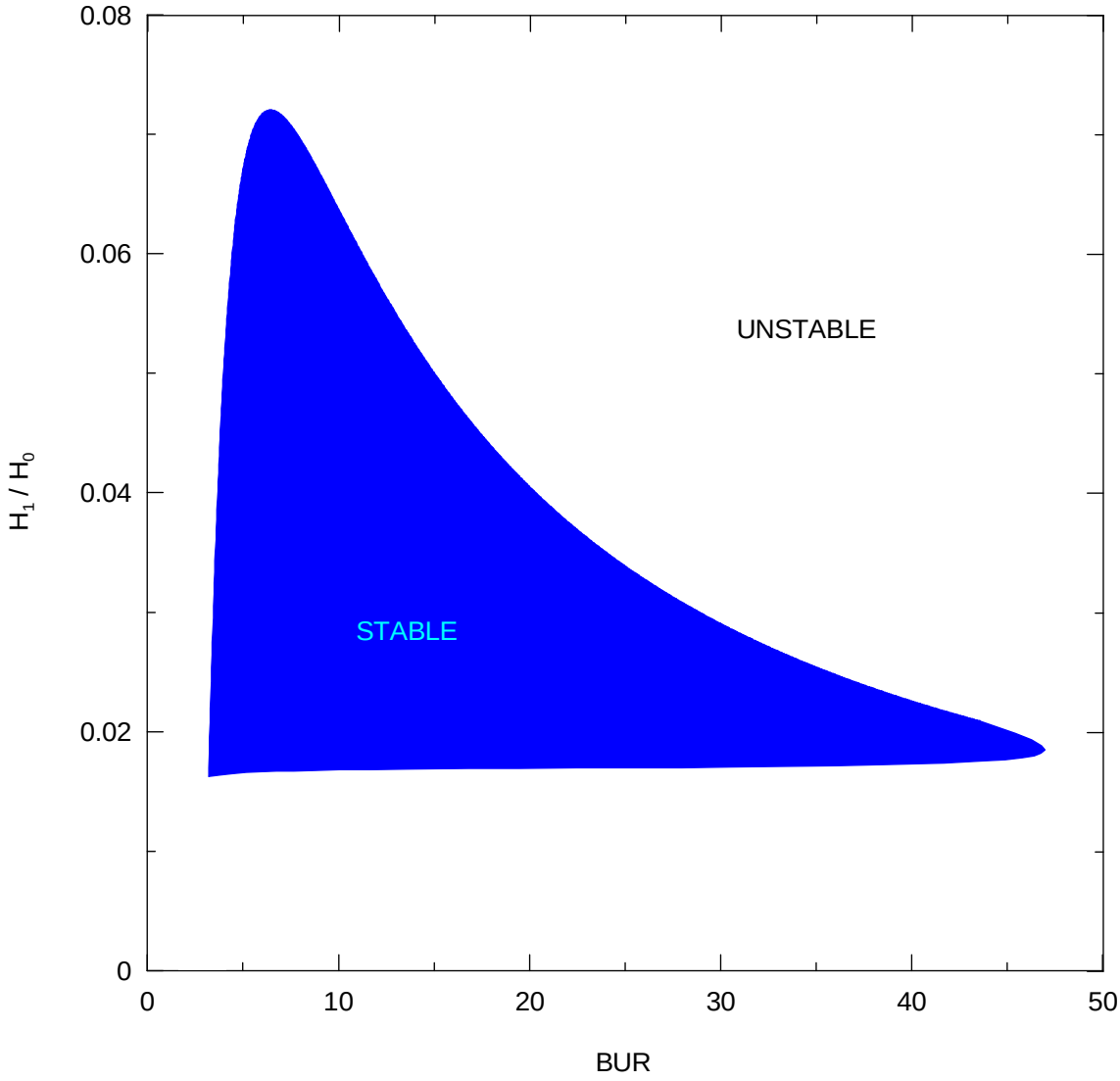

Fig. 17. Typical processing window predicted by the Zatloukal-Vlcek model for the Newtonian material (η_0 = 100 kPa·s, σ = 1 MPa) and the following processing conditions: L = 0.24 m, R_0 = 0.07282 m, Q = 43.40·10^{-7} m^3·s^{-1}, p = 90 Pa·m, H_0 = 1.34·10^{-3} m.

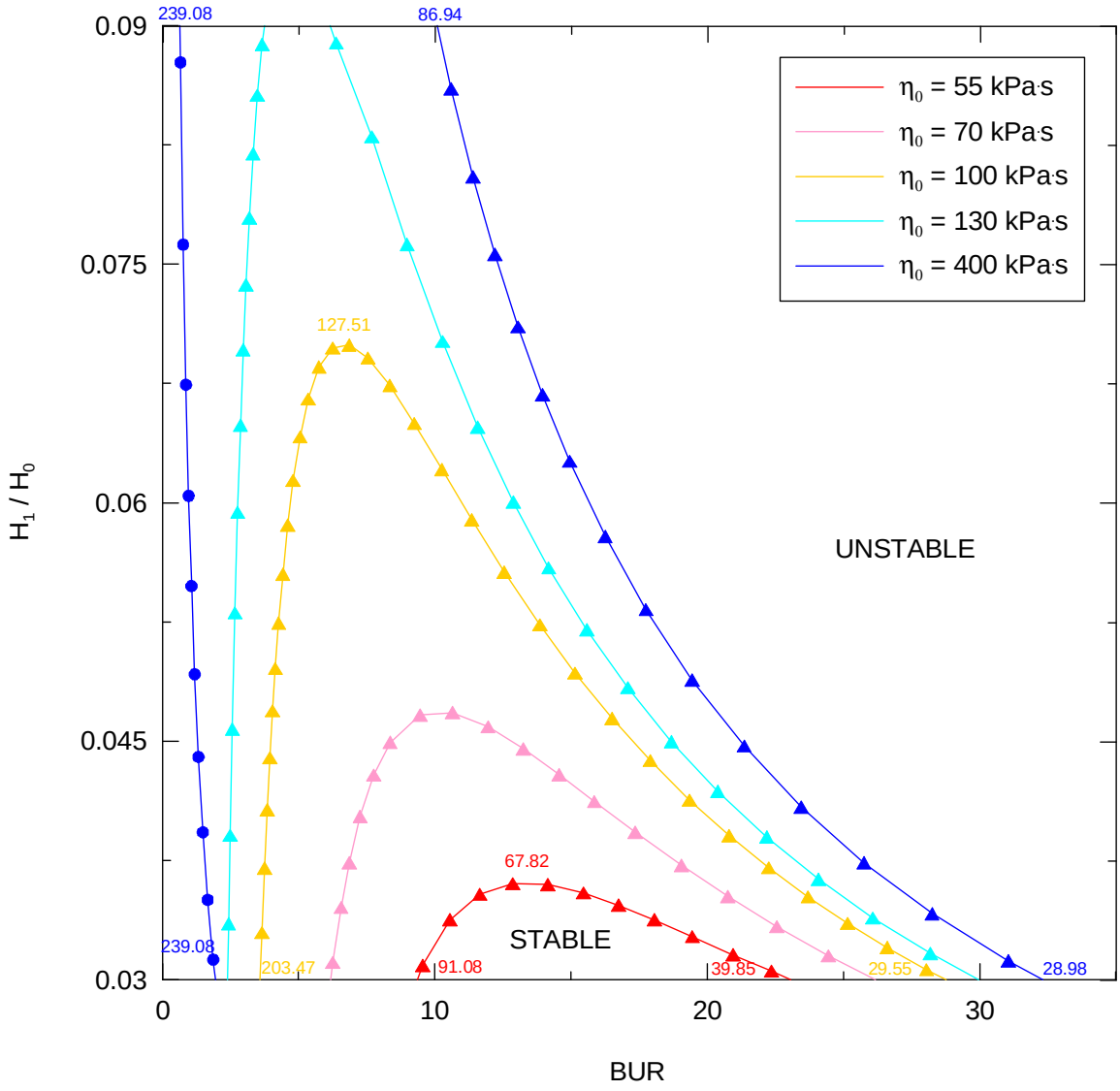

Fig. 18. Upper stability contours for different level of the Newtonian viscosity predicted by the Zatloukal-Vlcek model for Newtonian isothermal fluid ($\sigma = 1$ MPa) and fixed processing conditions (L = 0.18 m, R_0 = 0.037 m, Q = 43.40·10^{-7} m^3·s^{-1}, p = 111,163 Pa·m, H_0 = 1.34·10^{-3} m). Model and machine stability contours are represented by (▲) and (■), respectively.

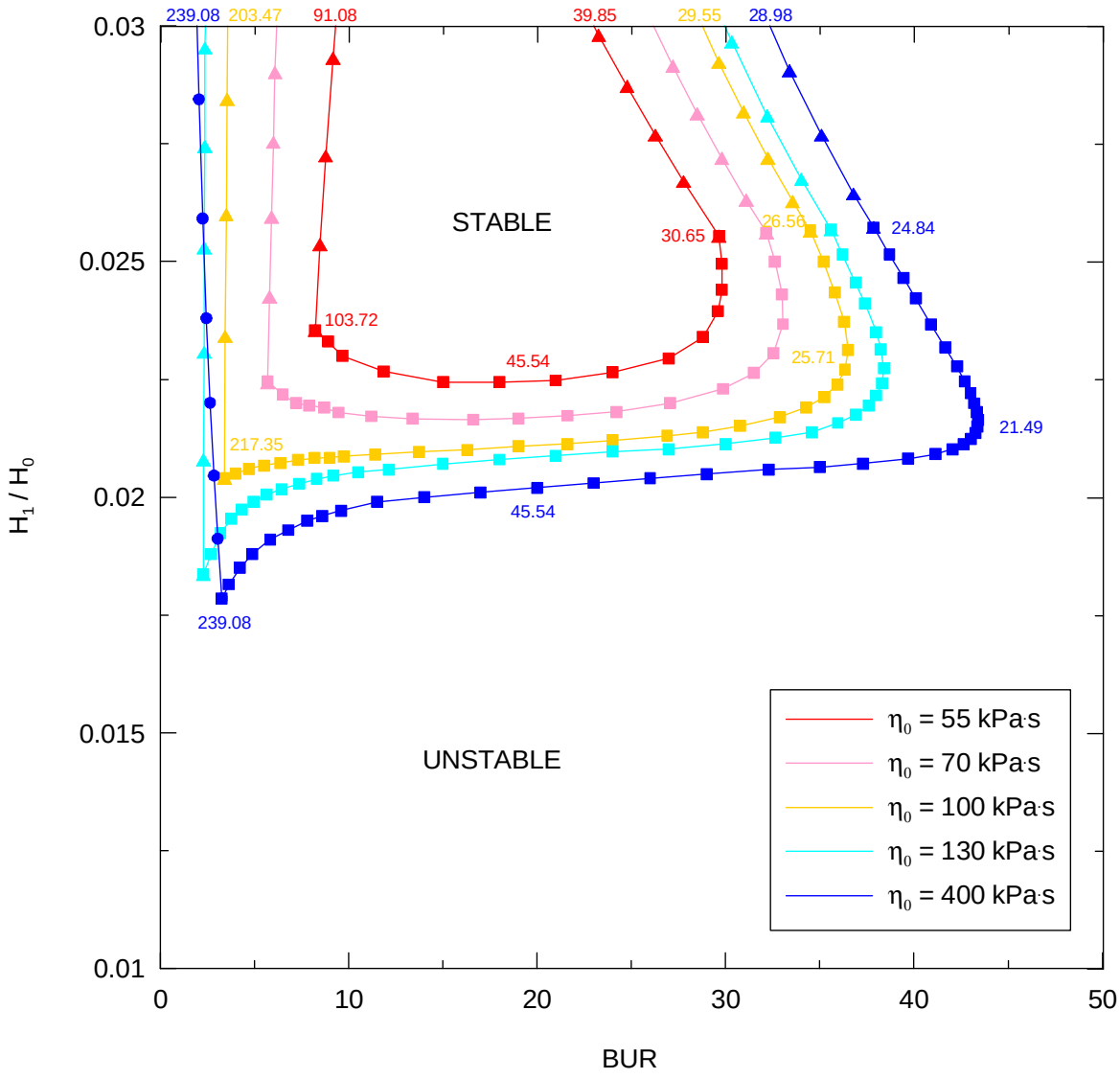

Fig. 19. Lower stability contours for different level of the Newtonian viscosity predicted by the Zatloukal-Vlcek model for Newtonian isothermal fluid ($\sigma = 1$ MPa) and fixed processing conditions (L = 0.18 m, R_0 = 0.037 m, Q = 43.40·10^{-7} m^3·s^{-1}, p = 111,163 Pa·m, H_0 = 1.34·10^{-3} m). Model, machine and circumference stability contours are represented by (▲), (■) and (■), respectively.

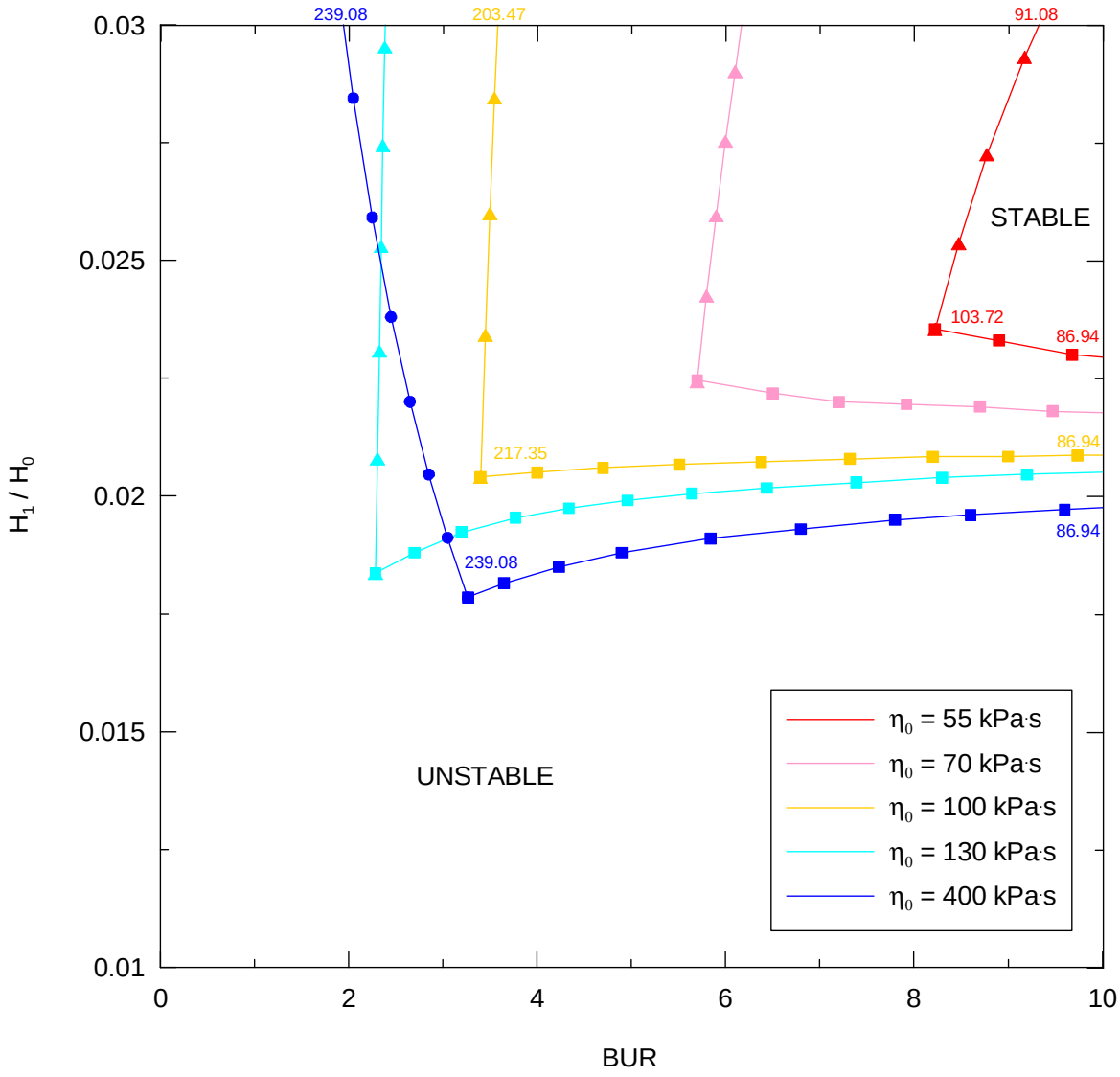

Fig. 20. Lower stability contours (BUR varies from 0 up to 10 only) for different level of the Newtonian viscosity predicted by the Zatloukal-Vlcek model for Newtonian isothermal fluid ($\sigma = 1$ MPa) and fixed processing conditions (L = 0.18 m, R_0 = 0.037 m, Q = 43.40·10^{-7} m^3·s^{-1}, p = 111,163 Pa·m, H_0 = 1.34·10^{-3} m). Model, machine and circumference stability contours are represented by (▲), (●) and (■), respectively.

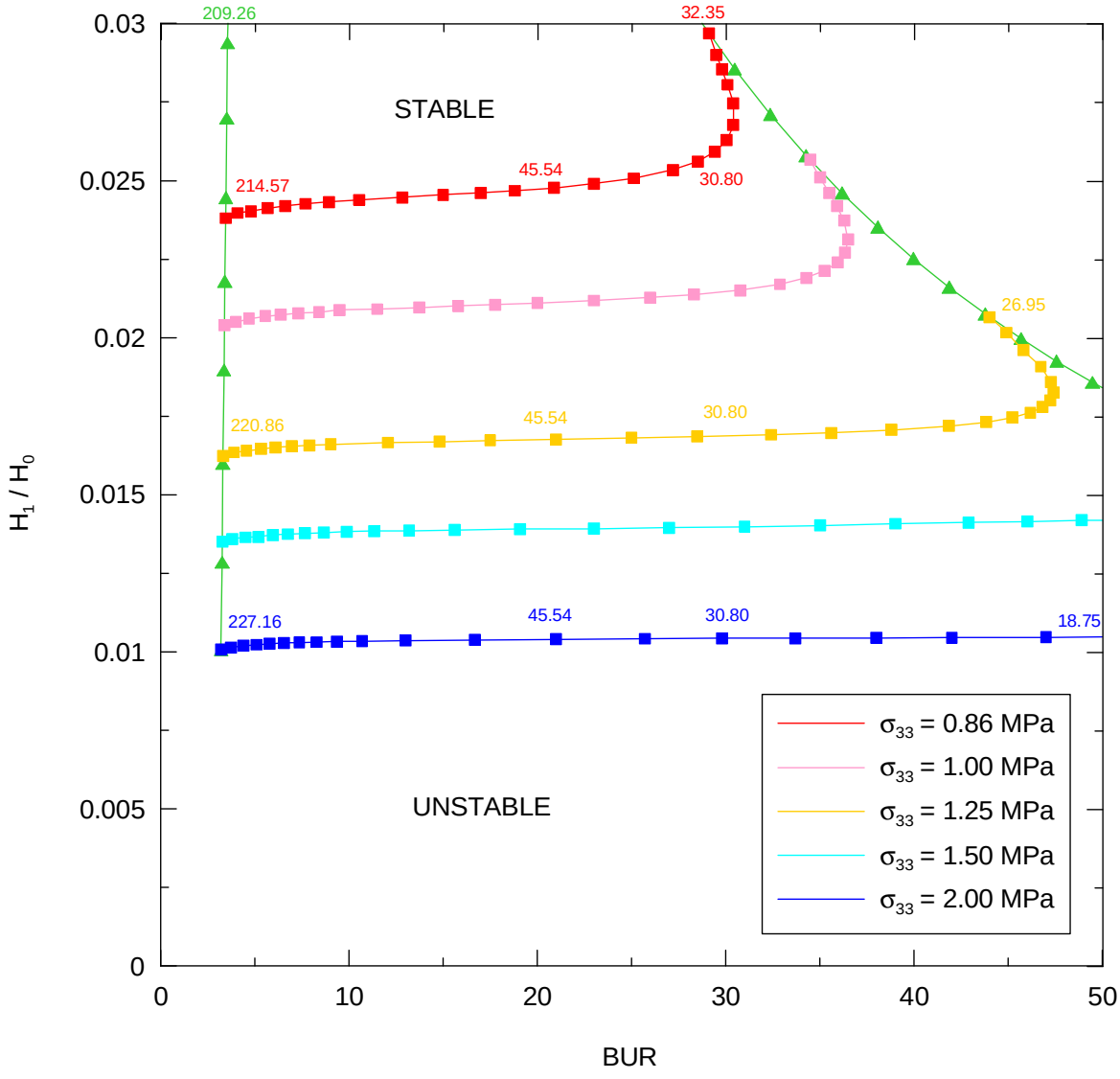

Fig. 21. Lower stability contours for different level of the melt strenght predicted by the Zatloukal-Vlcek model for Newtonian isothermal fluid (η_0 = 100 kPa·s) and fixed processing conditions (L = 0.18 m, R_0 = 0.037 m, Q = 43.40·10^{-7} m^3·s^{-1}, p = 111,163 Pa·m, H_0 = 1.34·10^{-3} m). Model and circumference stability contours are represented by (▲) and (■), respectively.

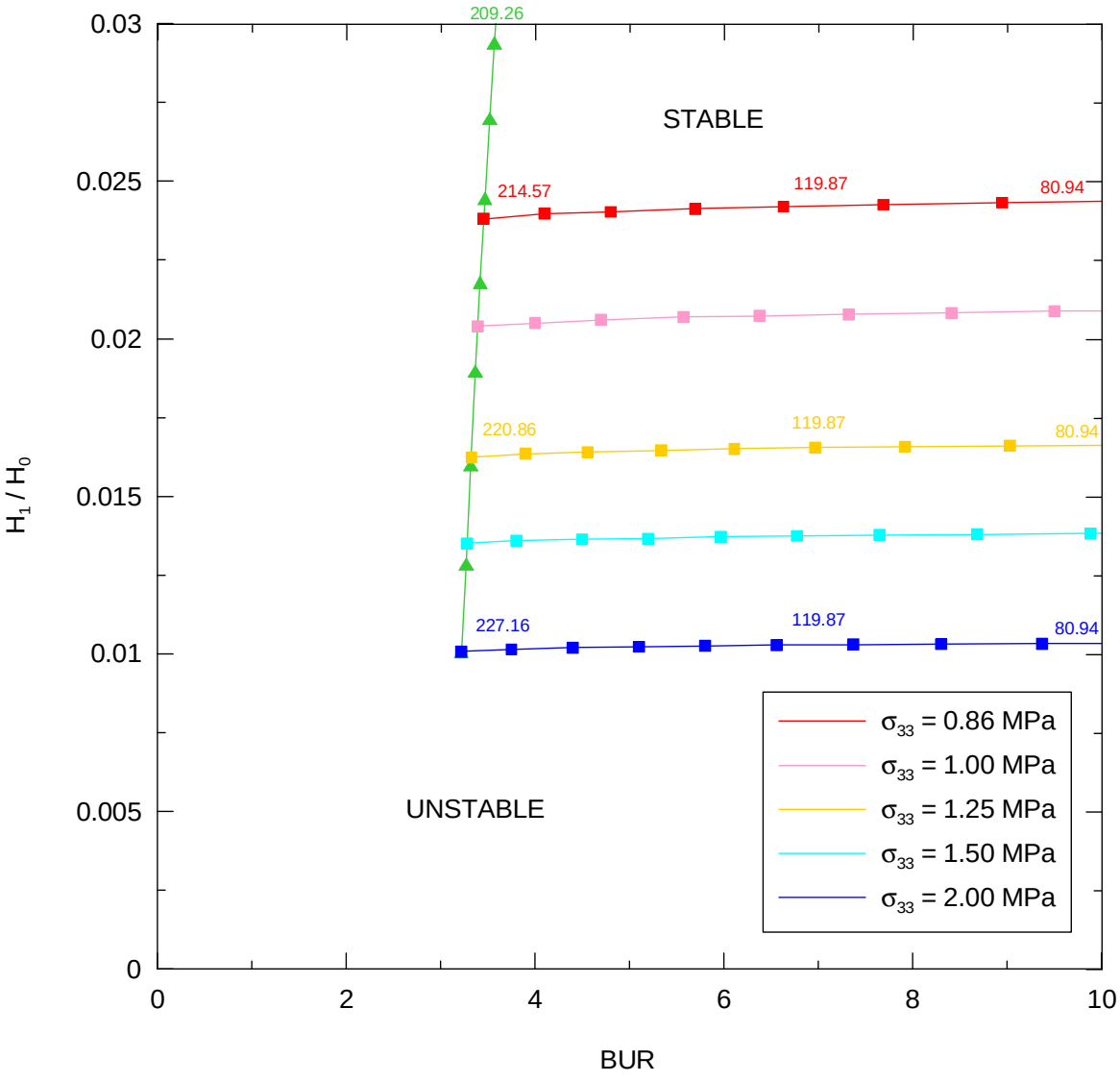

Fig. 22. Lower stability contours (BUR varies from 0 up to 10 only) for different level of the melt strenght predicted by the Zatloukal-Vlcek model for Newtonian isothermal fluid (η_0 = 100 kPa·s) and fixed processing conditions (L = 0.18 m, R_0 = 0.037 m, Q = 43.40·10^{-7} m^3·s^{-1}, p = 111,163 Pa·m, H_0 = 1.34·10^{-3} m). Model and circumference stability contours are represented by (▲) and (■), respectively.

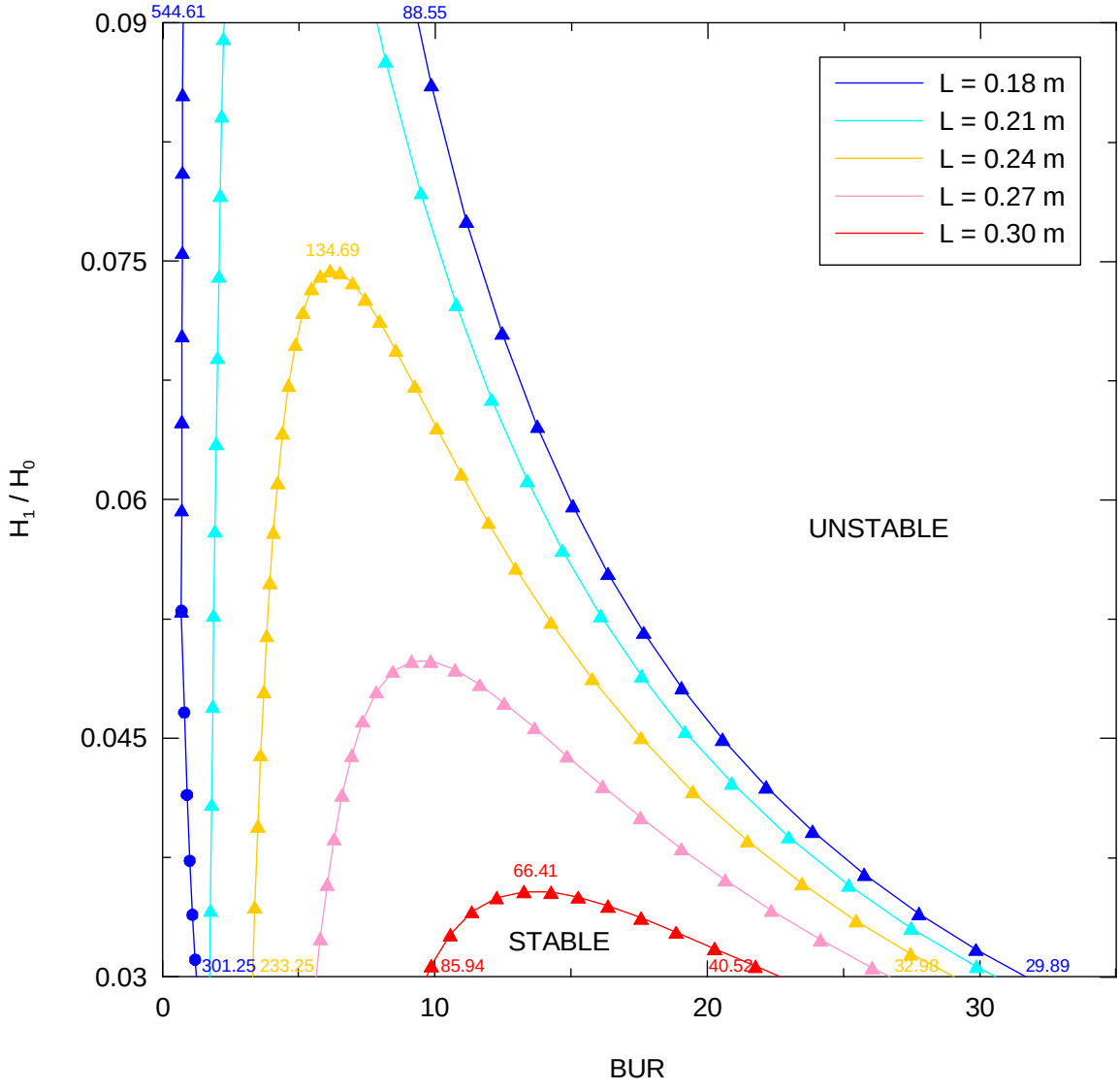

Fig. 23. Upper stability contours for different freeze line heights predicted by the Zatloukal-Vlcek model for Newtonian isothermal fluid (η_0 = 250 kPa·s, σ = 1 MPa) and the following processing conditions: R_0 = 0.037 m, Q = 43.40·10^{-7} m^3·s^{-1}, p = 111,163 Pa·m, H_0 = 1.34·10^{-3} m. Model and machine stability contours are represented by (▲) and (●), respectively.

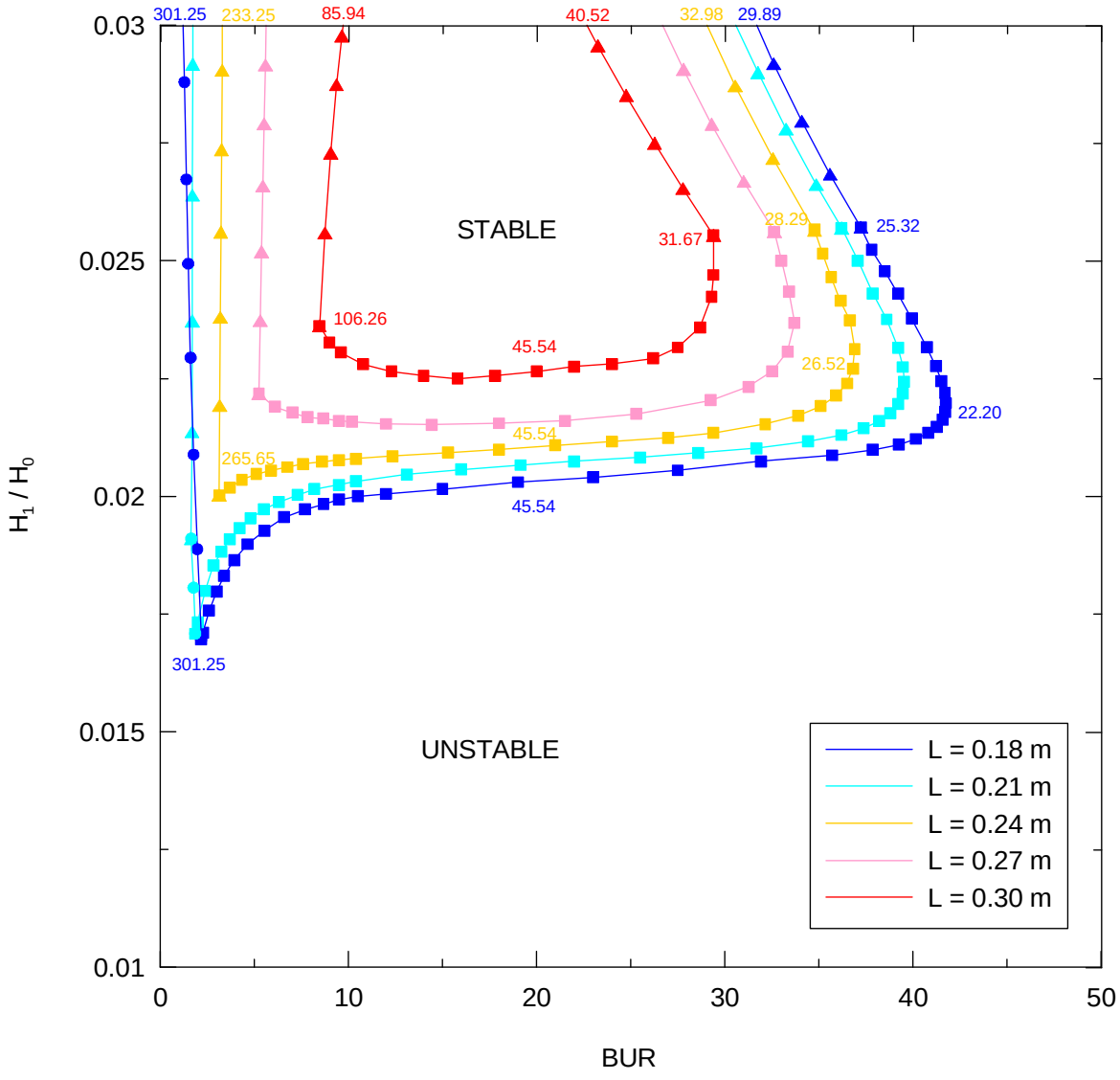

Fig. 24. Lower stability contours for different freeze line heights predicted by the Zatloukal-Vlcek model for Newtonian isothermal fluid (η_0 = 250 kPa·s, σ = 1 MPa) and the following processing conditions: R_0 = 0.037 m, Q = 43.40·10^{-7} m^3·s^{-1}, p = 111,163 Pa·m, H_0 = 1.34·10^{-3} m. Model, machine and circumference stability contours are represented by (▲), (●) and (■), respectively.

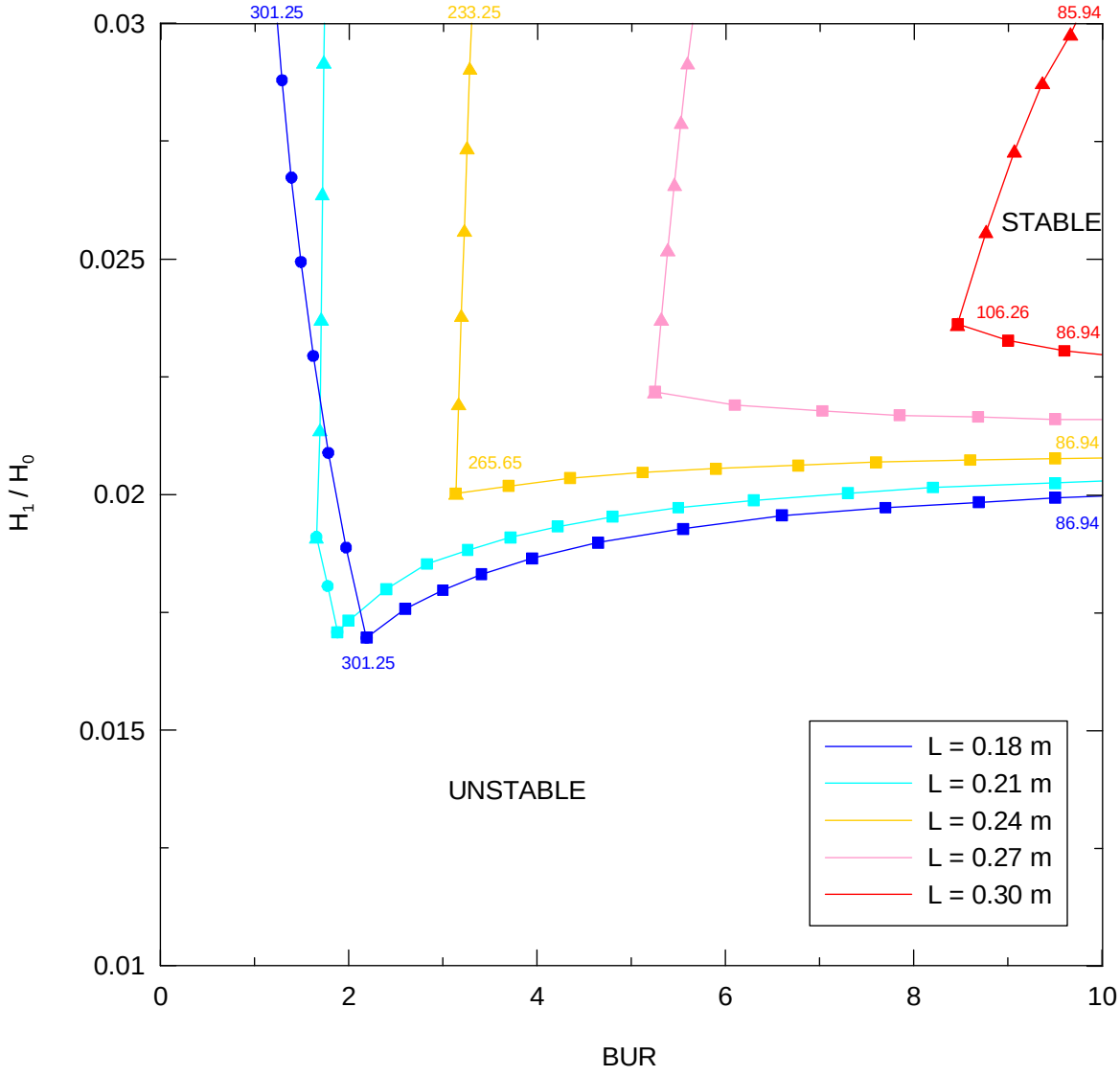

Fig. 25. Lower stability contours (BUR varies from 0 up to 10 only) for different freeze line heights predicted by the Zatloukal-Vlcek model for Newtonian isothermal fluid (η_0 = 250 kPa·s, σ = 1 MPa) and the following processing conditions: R_0 = 0.037 m, Q = 43.40·10^{-7} m^3·s^{-1}, p = 111,163 Pa·m, H_0 = 1.34·10^{-3} m. Model, machine and circumference stability contours are represented by (▲), (●) and (■), respectively.

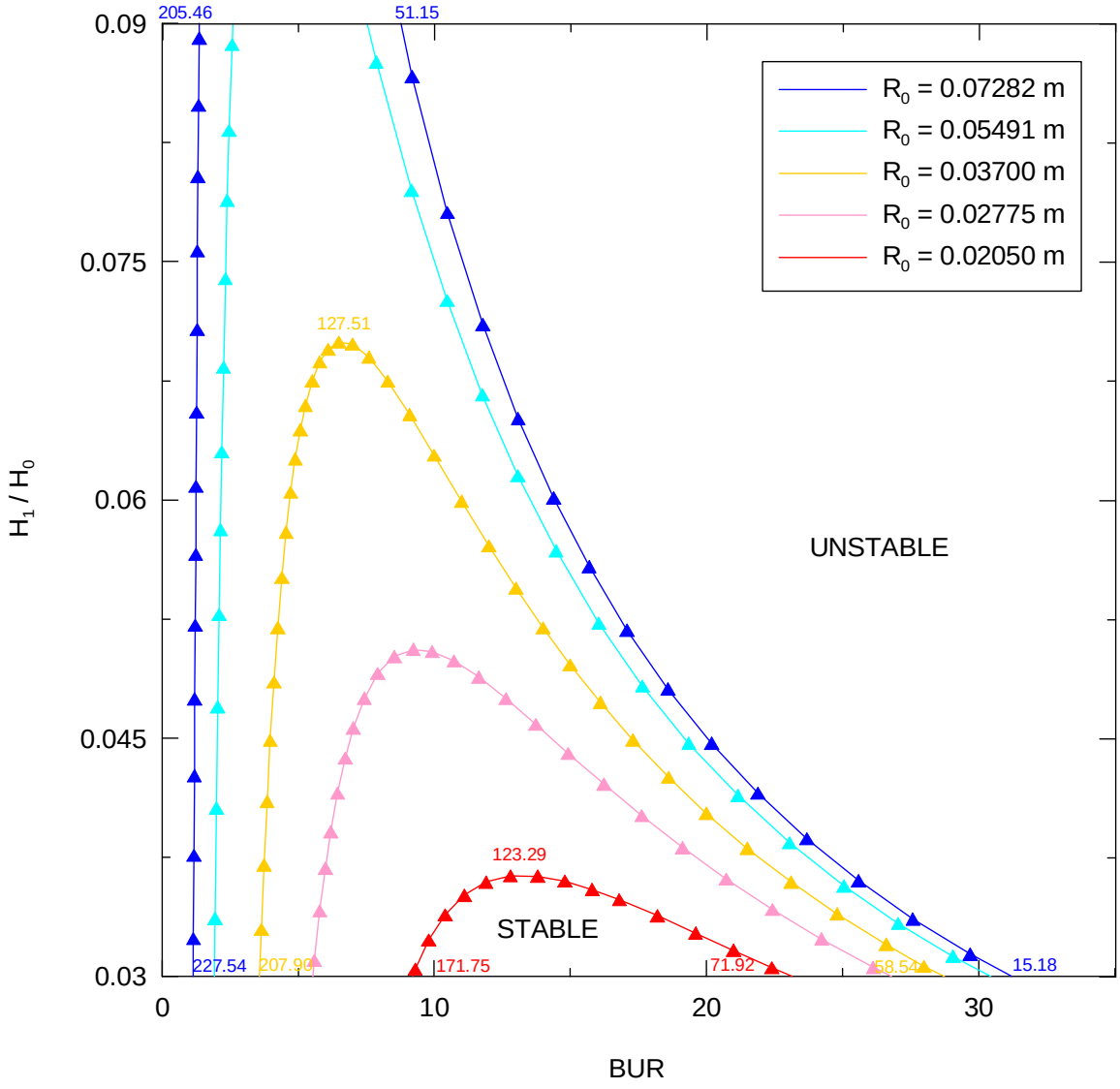

Fig. 26. Upper stability contours for different die radius predicted by the Zatloukal-Vlcek model for Newtonian isothermal fluid (η_0 = 100 kPa·s, σ = 1 MPa) and the fixed processing conditions (L = 0.18 m, Q = 43.40·10^{-7} m^3·s^{-1}, p = 111,163 Pa·m, H_0 = 1.34·10^{-3} m). Model stability contours are represented by (▲).

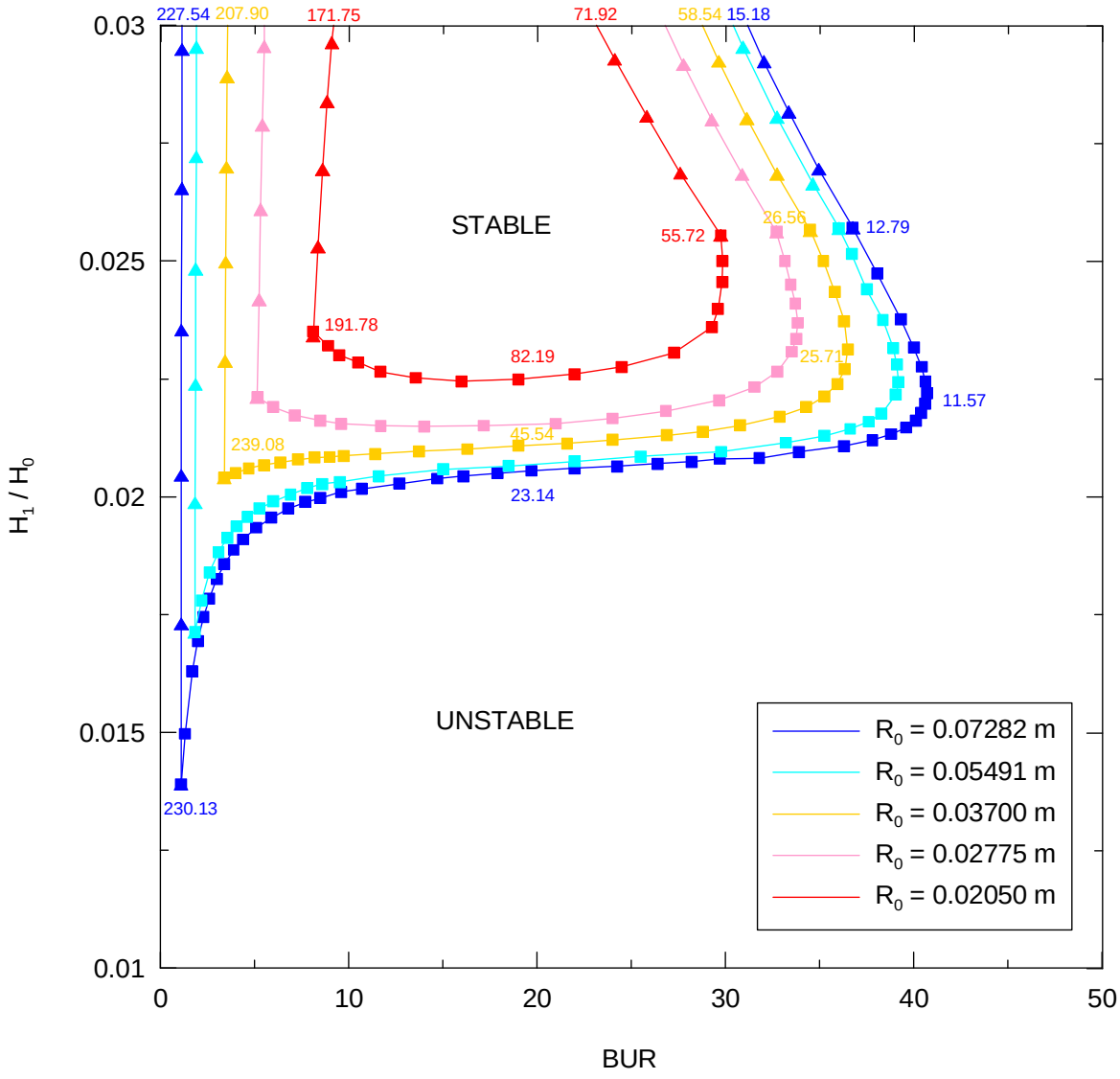

Fig. 27. Lower stability contours for different die radius predicted by the Zatloukal-Vlcek model for Newtonian isothermal fluid (η_0 = 100 kPa·s, σ = 1 MPa) and the fixed processing conditions (L = 0.18 m, Q = 43.40·10^{-7} m^3·s^{-1}, p = 111,163 Pa·m, H_0 = 1.34·10^{-3} m). Model and circumference stability contours are represented by (▲) and (■), respectively.

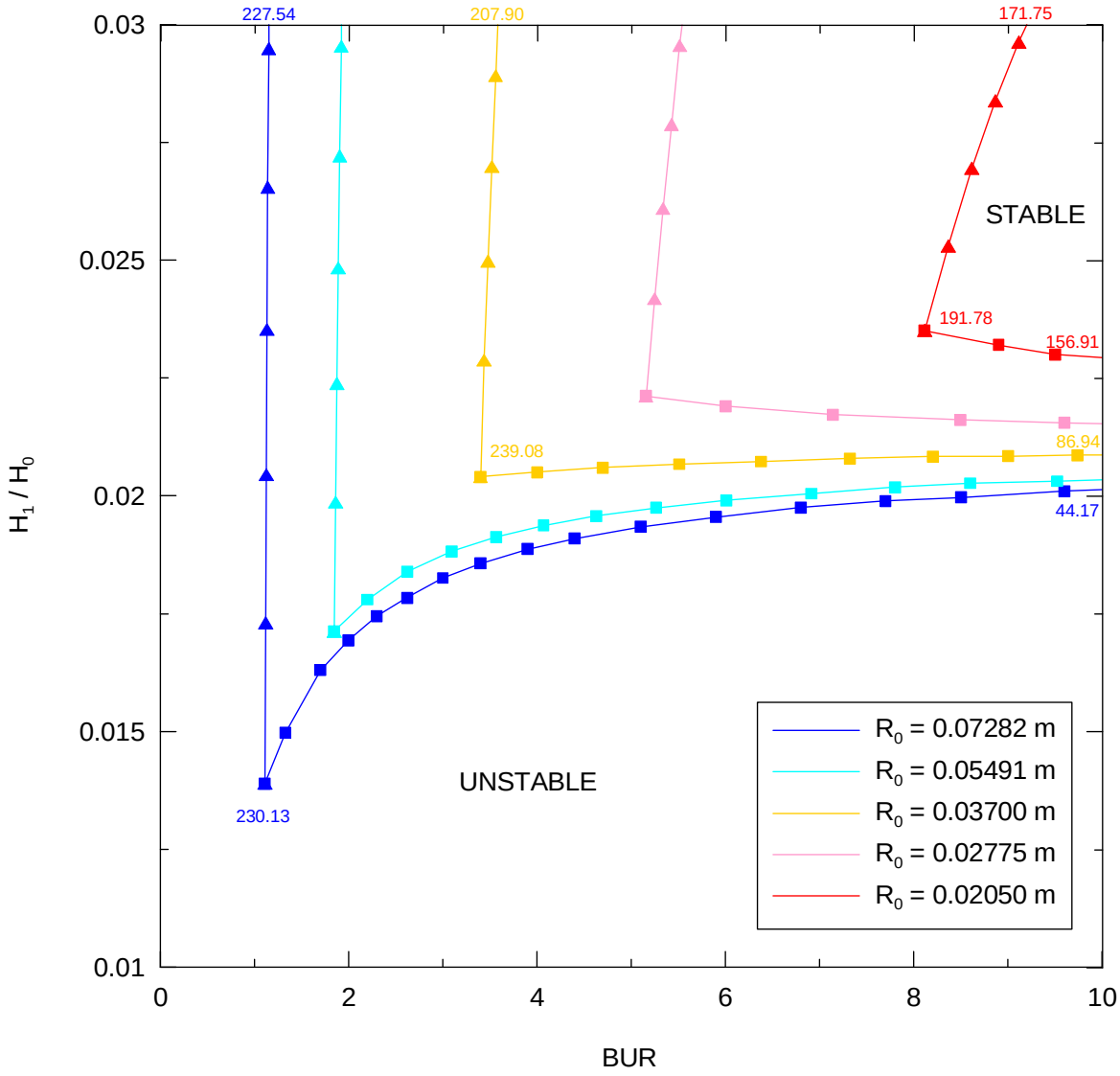

Fig. 28. Lower stability contours (BUR varies from 0 up to 10 only) for different die radius predicted by the Zatloukal-Vlcek model for Newtonian isothermal fluid (η_0 = 100 kPa·s, σ = 1 MPa) and the fixed processing conditions (L = 0.18 m, $Q = 43.40 \cdot 10^{-7}$ $m^3 \cdot s^{-1}$, p = 111,163 Pa·m, $H_0 = 1.34 \cdot 10^{-3}$ m). Model and circumference stability contours are represented by (▲) and (■), respectively.

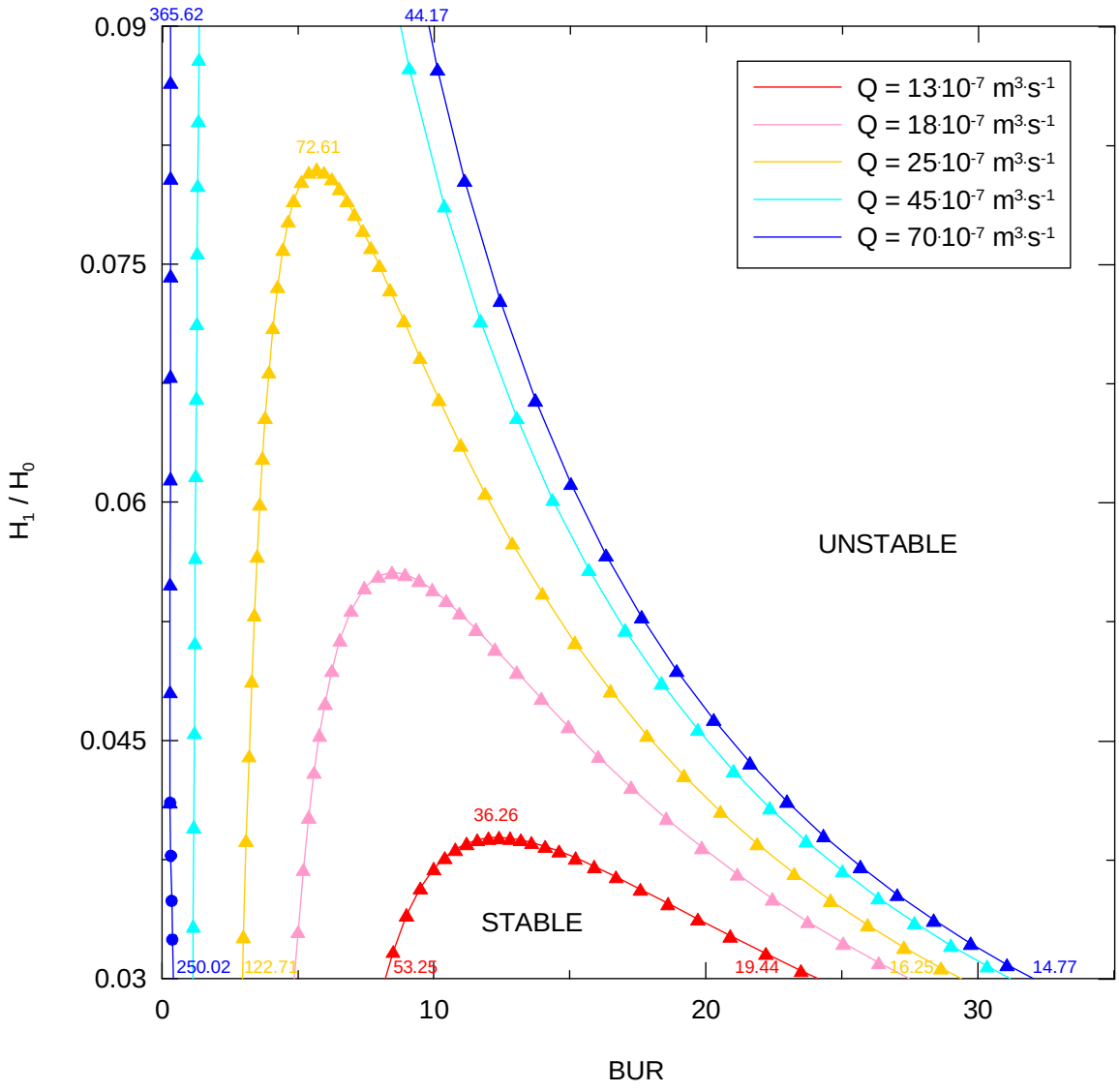

Fig. 29. Upper stability contours for different volume flow rates predicted by the Zatloukal-Vlcek model for Newtonian isothermal fluid (η_0 = 100 kPa·s, σ = 1 MPa) and the following processing conditions: R_0 = 0.07282 m, L=0.18 m, p = 111,163 Pa·m, $H_0 = 1.34 \cdot 10^{-3}$ m. Model and machine stability contours are represented by (▲) and (●), respectively.

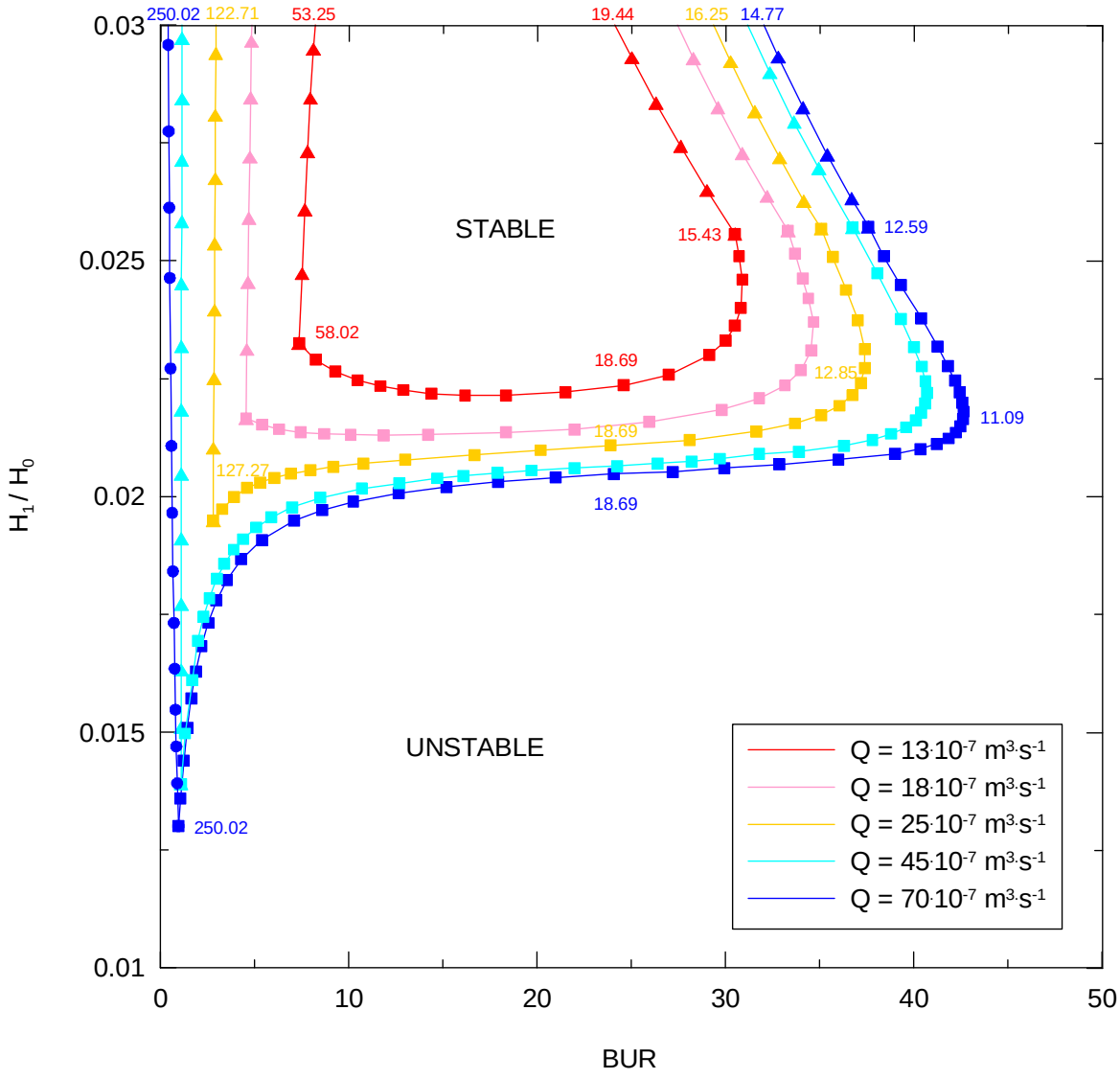

Fig. 30. Lower stability contours for different volume flow rates predicted by the Zatloukal-Vlcek model for Newtonian isothermal fluid (η_0 = 100 kPa·s, σ = 1 MPa) and the following processing conditions: R_0 = 0.07282 m, L=0.18 m, p = 111,163 Pa·m, H_0 = 1.34·10^{-3} m. Model, machine and circumference stability contours are represented by (▲), (●) and (■), respectively.

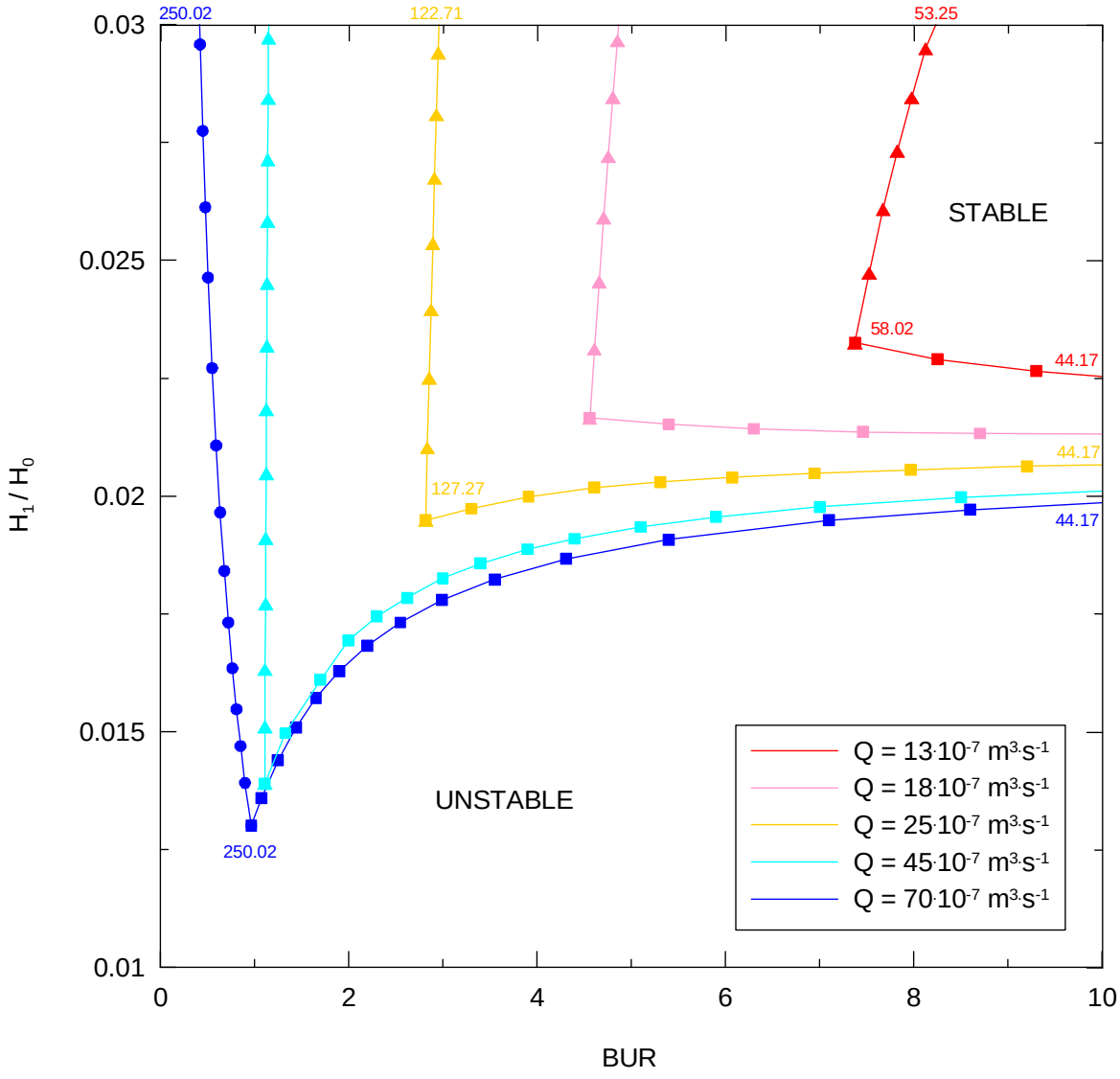

Fig. 31. Lower stability contours (BUR varies from 0 up to 10 only) for different volume flow rates predicted by the Zatloukal-Vlcek model for Newtonian isothermal fluid (η_0 = 100 kPa·s, σ = 1 MPa) and the following processing conditions: R_0 = 0.07282 m, L=0.18 m, p = 111,163 Pa·m, H_0 = 1.34·10^{-3} m. Model, machine and circumference stability contours are represented by (▲), (●) and (■), respectively.

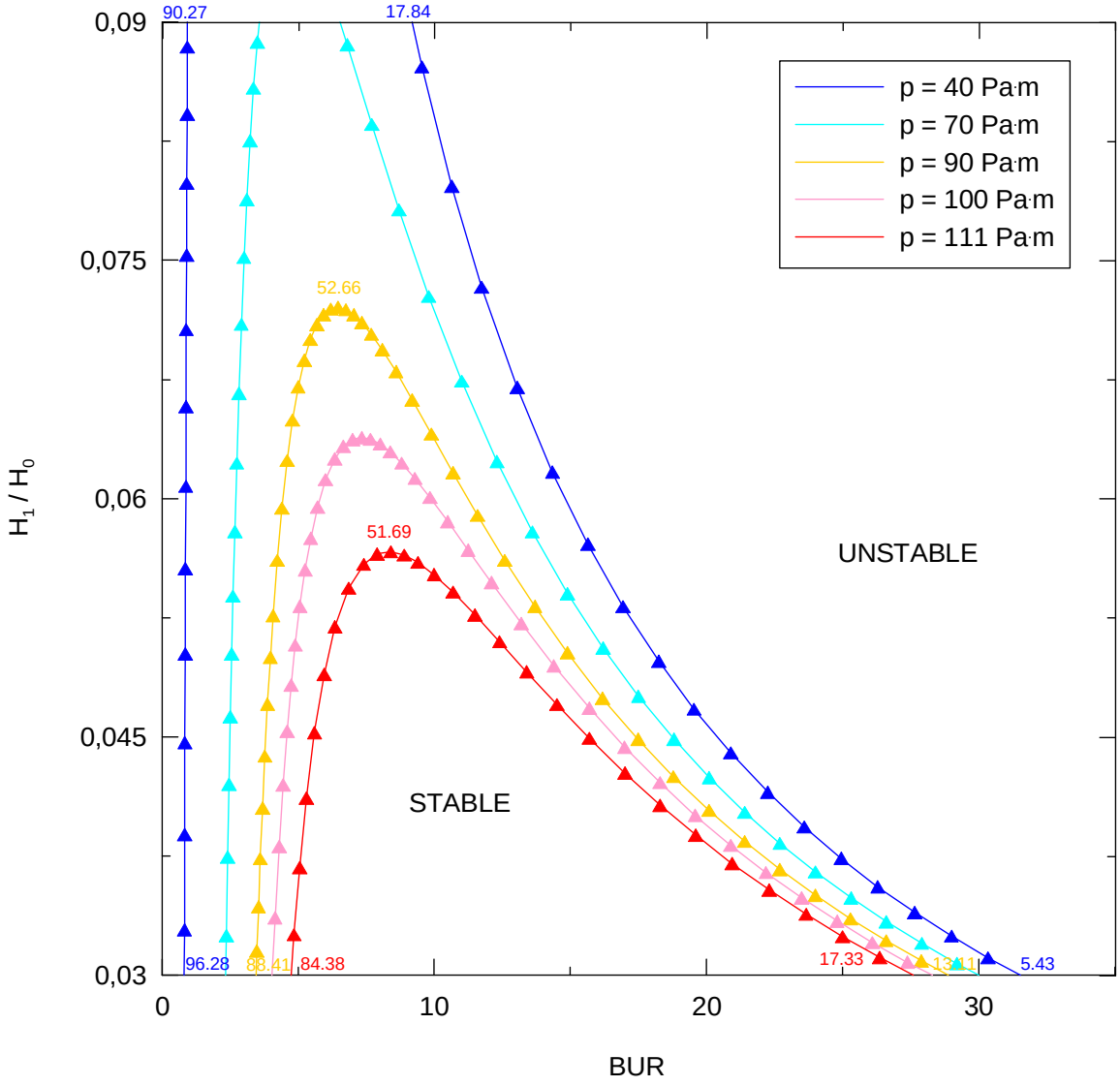

Fig. 32. Upper stability contours for different level of the internal load predicted by the Zatloukal-Vlcek model for Newtonian isothermal fluid (η_0 = 100 kPa·s, σ = 1 MPa) and fixed processing conditions (L = 0.24 m, R_0 = 0.07282 m, Q = 43.40·10^{-7} m^3·s^{-1}, H_0 = 1.34·10^{-3} m). Model contours are represented by (▲).

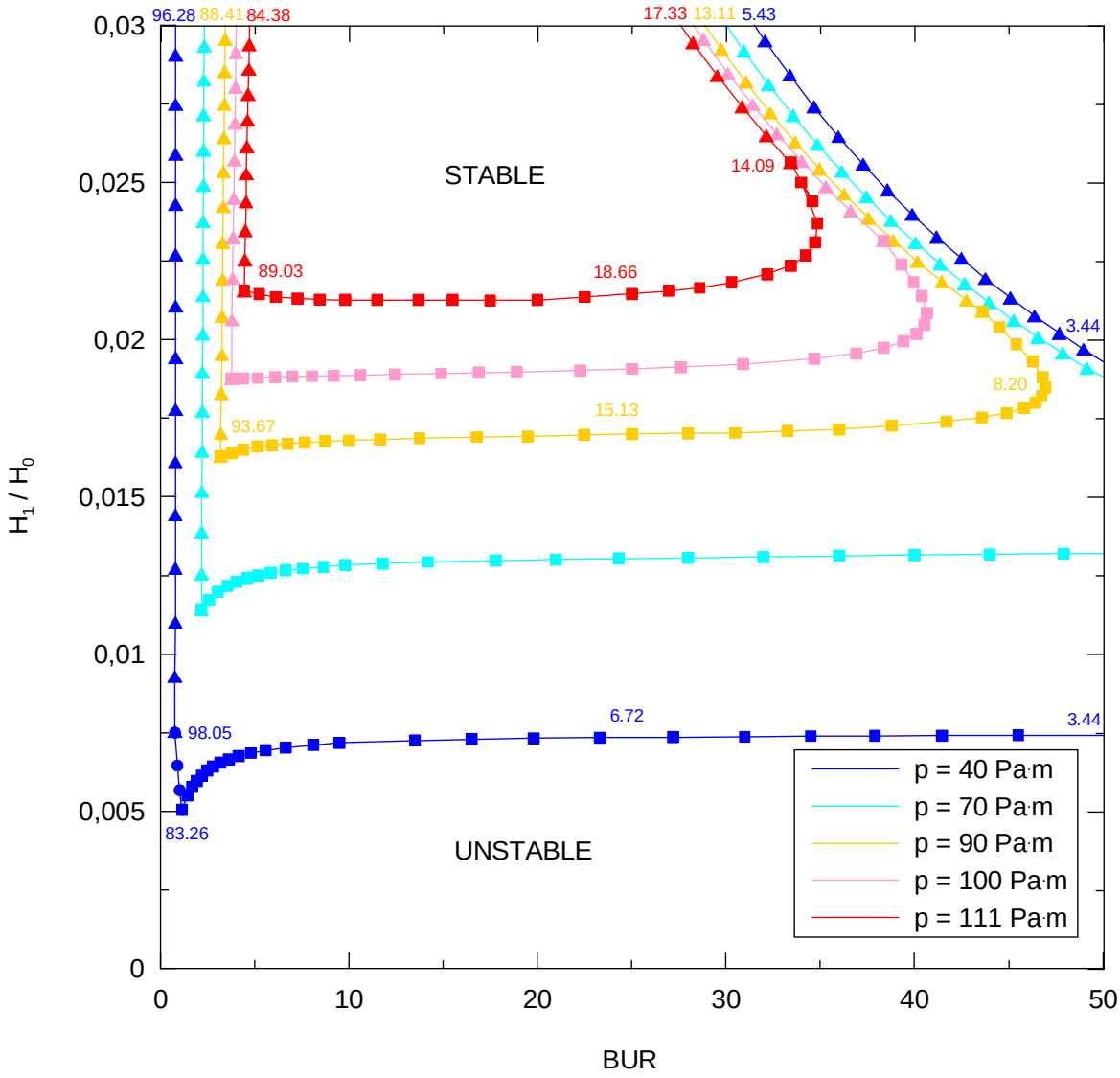

Fig. 33. Lower stability contours for different level of the internal load predicted by the Zatloukal-Vlcek model for Newtonian isothermal fluid (η_0 = 100 kPa·s, σ = 1 MPa) and fixed processing conditions (L = 0.24 m, R_0 = 0.07282 m, $Q = 43.40 \cdot 10^{-7}$ $m^3 \cdot s^{-1}$, $H_0 = 1.34 \cdot 10^{-3}$ m). Model, machine and circumference stability contours are represented by (▲), (●) and (■), respectively.

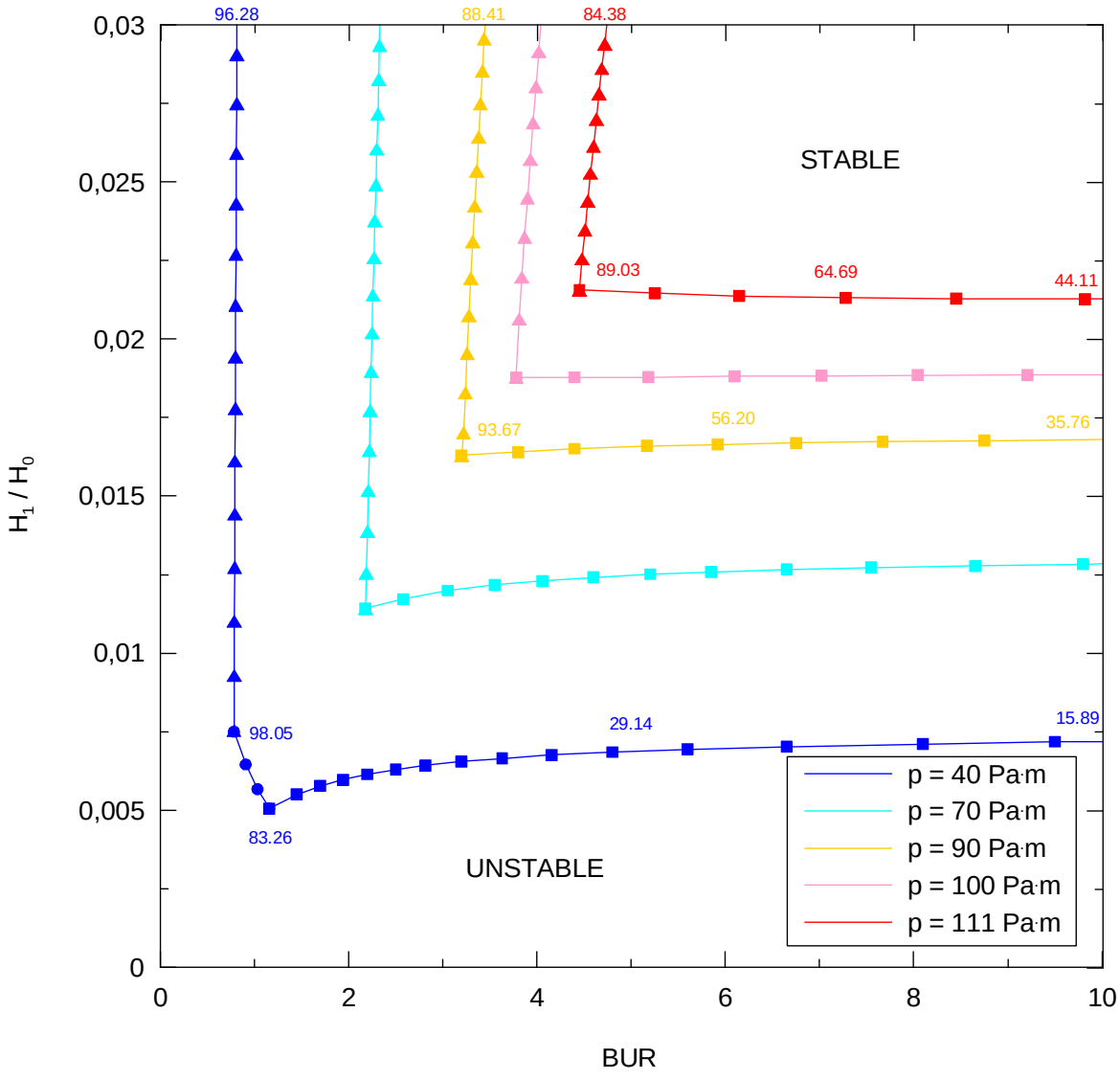

Fig. 34. Lower stability contours (BUR varies from 0 up to 10 only) for different level of the internal load predicted by the Zatloukal-Vlcek model for Newtonian isothermal fluid (η_0 =100 kPa·s, σ=1 MPa) and fixed processing conditions (L = 0.24 m, R_0 = 0.07282 m, Q = 43.40·10^{-7} m^3·s^{-1}, H_0 = 1.34·10^{-3} m). Model, machine and circumference stability contours are represented by (▲), (●) and (■), respectively.

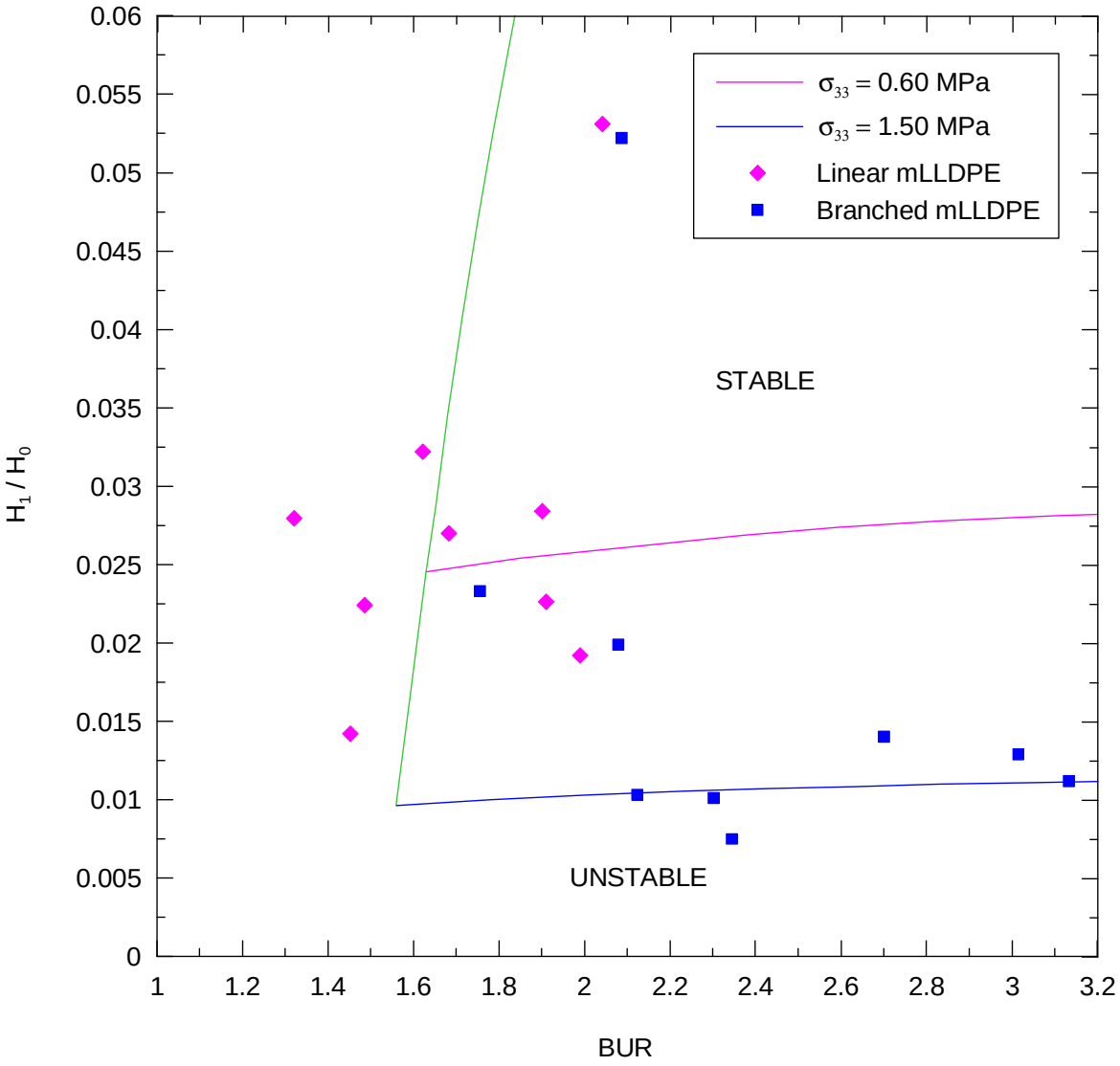

Fig. 35. Comparison between experimentally determined stability points and theoretical stability contours predicted by the Zatloukal-Vlcek model for Newtonian isothermal fluids (η_0 = 146 kPa·s) and following processing conditions: L = 0.18 m, R_0 = 0.037 m, Q = 43.40·10^{-7} m^3·s^{-1}, p = 100 Pa·m, H_0 = 1.34·10^{-3} m.

REFERENCES

[1] TAS. P. P.: *Film blowing from polymer to product*, Ph.D. Thesis, Technische Universitat Eindhoven, 1994.

[2] LUO, X. L., TANNER, R. I.: *A computer study of film blowing*, Polym. Eng. Sci. 25, p. 620, 1985.

[3] ASHOK, B. K., CAMPBELL, G. A.: *2-Phase simulation of tubular film blowing of crystalline polymers*, Int. Polym. Proc. 7, p. 240, 1992.

[4] ZATLOUKAL, M., SAHA, P.: *Modeling of the film blowing process by using variational principles for high stalk bubbles*, PPS-21, Leipzig, Germany, 2005 (CD-ROM).

[5] ZATLOUKAL, M., VLCEK, J.: *Modeling of the film blowing process by using variational principles*, J. Non-Newtonian Fluid Mech. 123, p. 201-213, 2004.

[6] ZATLOUKAL, M., VLCEK, J.: *Application of variational principles in modeling of the film blowing process for high stalk bubbles*, J. Non-Newtonian Fluid Mech. 133, p. 63-72, 2006.

[7] ZATLOUKAL, M., MAVRIDIS, H., VLCEK, J., SAHA, P.: *Modeling of Non-isothermal Film Blowing Process by Using Variational Principles*. SPE ANTEC, p. 825-829, Charlotte, USA, 2006.

[8] KANAI, T., CAMPBELL, G. A.: *Film Processing: Progress in Polymer Processing*, Hanser Gardner Publications, Munich, Germany, 1999.

[9] AGASSANT, J. F., AVENAS, P., SERGENT, J. Ph., CARREAU, P. J.: *Polymer processing: Principles and modeling*, Carl Hanser, Munich, Gremany, 1991.

[10] BUTLER, T. I.: *Blown film bubble instability induced by fabrication conditions*, SPE ANTEC Tech. Papers 1, p. 1120, 2000.

[11] HAN, C. D., PARK, J. Y.: *Studies on blown film extrusion: Part 3. Bubble instability*, J. Appl. Polymer Sci. 19, p. 3291, 1975.

[12] HAN, C. D., SHETTY, R.: *Flow instability in tubular film blowing: Part 1. Experimental study*, Ind. Eng. Chem. Fund., 16, p. 49, 1977.

[13] OBIJESKI, T. J., PURITT, K. R.: *Improving the output and bubble stability of thick gauge blown film*, SPE ANTEC Tech. Papers 1, p. 150, 1992.

[14] KANAI, T., WHITE, J. L.: *Kinematics, dynamics and stability of the tubular film extrusion of various polyethylenes*, J. Non-Newtonian Fluid Mech. 19, p. 275, 1986.

[15] SWEENEY, P. A., CAMPBELL, G. A.: *Blown film stability*, ANTEC 461, 1993.

[16] LAFUENTE-CANAS, P., FERNÁNDEZ AMO, B., SMITH, G. D., SPARES, R., MARTYN, M. T., COATES, P. D.: *Blown Film: processing stability for metallocenes*, in: Polymer Process Engineering 03: Enhanced Polymer Processing, p. 192-213. Edited by PD Coates, University Press, Bradford, UK, 2003

[17] MUKE, S., CONNELL, H., SBARSKI, I., BHATTACHARYA, S. N.: *Numerical modeling and experimental verification of blown film processing*, J. Non-Newtonian Fluid Mech. 116, p. 113-138, 2003.

[18] PEARSON, J. R., PETRIE, C. J. S.: *The flow of a tubular film. Part 2. Interpretation of the model and discussion of solutions*, J. Fluid Mech. 42, p. 60, 1970.

[19] PEARSON, J. R. A., PETRIE, C. J. S.: *The flow of a tubular film. Part 1. Formal mathematical representation*, J. Fluid Mech. 40, p. 1, 1970.

[20] PETRIE, C. J. S.: *A comparison of theoretical predictions with published experimental measurements on the blown film process*, Am. Inst. Chem. Eng. J. 21, p. 275, 1975.

[21] HAN, C. D., PARK, J. Y.: *Studies on blown film extrusion. 2. Analysis of the deformation and heat transfer process*, J. Appl. Polym. Sci. 19, p. 3277-3290, 1975.

[22] WAGNER, M. H.: *Das folienblasverfahren als rheologish-thermodynamischer PozeB*, Rheol. Acta 15, p. 40-51, 1976.

[23] PEARSON, J. R., GUTTERIDGE, P. A.: *Stretching flow for thin film production. Part 1. Bubble blowing in the solid phase*, J. Non-Newtonian Fluid Mech. 4, p. 57-72, 1978.

[24] KANAI, T., WHITE, J. L.: *Dynamics, heat transfer and structure development in tubular film extrusion of polymer melts: a mathematical model and predictions*, J. Polym. Eng. 5, p. 135, 1985.

[25] CAIN, J. J., DENN, M. M.: *Multiplicities and instabilities in film blowing*, Polym. Eng. Sci. 28, p. 1527, 1988.

[26] CAMPBELL, G. A., CAO, B.: *Blown film simulation, A severe test for rheological models*, in: Collyer, A.A.a.U.L.A. (Ed.), Polymer Rheology and Processing, Elsevier, Amsterdam, 1990.

[27] CAO, B., CAMPBELL, G. A.: *Viscoplastic-elastic modeling of tubular blown film processing*, Am. Inst. Chem. Eng. J. 36, p. 420, 1990.

[28] ALAIE, S. M., PAPANASTASIOU, T. C.: *Modeling of non-isothermal film blowing with integral constitutive equations*, Int. Polym. Process. 8, p. 51-65, 1993.

[29] LIU, C. C., BOQUE, D. C., SPRUIELL J. E.: *Tubular film blowing. Part 2. Theoretical modeling*, Int. Polym. Process. 10, p. 230, 1995.

[30] SIDIROPOULOS, V., VLACHOPOULOS, J.: *Computer simulation of film blowing*, in: Proceeding of the ANTEC, 1996.

[31] SIDIROPOULOS, V., TIAN, J. J., VLACHOPOULOS, J.: *Computer simulation of film blowing*, TAPPI J. 79, p. 113-118, 1996 .

[32] SPENCER, R. S., GILMORE, R. D.: J. Appl. Phys., p. 21-523, 1950.

[33] HELLWEGE, K. H., KNAPPE, W., LEHMANN, P., KOLLOID, Z.: Polymere 183, p. 110-120, 1962.

[34] FISHER, E.: *Ein Rheologisches Modell zur Beschreibung der Produktqualität bei der Verarbeitung von Hochdruckpolyethylen*, Ph.D. thesis, IKT Stuttgart, Germany, 1983.

[35] MUSIL, J.: *The effect of long chain branching on processibility of polymer melts*, Bc. Thesis, Tomas Bata University in Zlín, Czech Republic, 2006.

LIST OF SYMBOLS

BUR	Blow-up ratio	1
R_1	Bubble radius at the freeze line height FLH	m
R_0	Bubble radius at the die exit	m
DDR	Draw down ratio	1
v_F	Film velocity at the freeze line height	$m \cdot s^{-1}$
v_D	Film velocity at the die exit	$m \cdot s^{-1}$
$Q´$	Mass flow rate	$kg \cdot s^{-1}$
π	Ludolf´s number	1
r	Bubble radius	m
h	Film thickness	m
v	Film velocity	$m \cdot s^{-1}$
ρ	Film density	$kg \cdot m^{-3}$
R_g	Universal gas constant	$J \cdot K^{-1} mol^{-1}$
T	Temperature	K
P^*	Cohesion pressure	Pa
w	Molecular weight	$kg \cdot mol^{-1}$
$b´$	Specific volume	$m^3 \cdot kg^{-1}$
Δp	Internal bubble pressure	Pa
L	Freeze line height FLH	m
σ_{11}	Tangential component of the total stress tensor	Pa
R_m	Curvature radius	m
σ_{33}	Circumferential component of the total stress tensor	Pa
R_t	Curvature radius	m
Θ	Bubble angle	°

F	Take-up force	N
G	Gravity	N
H	Force created by the air flow	N
r_f	Bubble radius at the freeze line height	m
H_1	Bubble thickness at the freeze line height	m
dx	Element length in x direction	m
dr	Element length in r direction	m
σ	Total stress tensor	Pa
p	Internal load	Pa·m
I	Unit tensor	1
τ	Extra stress	Pa
σ_{22}	Thickness directions of the stress	Pa
τ_{11}	Extra stress in the tangential directions	Pa
τ_{22}	Extra stress in the thickness directions	Pa
τ_{33}	Extra stress in the circumferential directions	Pa
J	Membrane compliance	Pa^{-1}
y	Equation for the bubble shape (radius) without the neck	m
λ_1	Lagrange multiplier	Pa
pJ	Film blowing model parameter	m
φ	Zatloukal-Vlcek model function	1
A	Zatloukal-Vlcek model function	1
$\alpha´$	Zatloukal-Vlcek model function	1
$\varphi´´$	Zatloukal-Vlcek model function	1
$A´´$	Zatloukal-Vlcek model function	1
$\alpha´´$	Zatloukal-Vlcek model function	1

BUR_0	Blow-up ratio at the neck	1
y_1, y_2	Equations for the bubble shape (radius) having the neck height	m
L_1	Neck height	m
ξ	Zatloukal-Vlcek model function	m^2
F_I	Tensile force acting at the die exit (Zatloukal-Vlcek model)	N
F_{II}	Tensile force at the freeze line height (Zatloukal-Vlcek model)	N
pL	Force acting in the thickness direction	N
Q	Volumetric flow rate	$m^3 \cdot s^{-1}$
η_0	Newtonian viscosity	Pa·s
D	Deformation rate tensor	s^{-1}
$F_{II,N}$	Force acting at the freeze line height (Newton model)	N
$\dot{\varepsilon}_1$	Extensional strain rate	s^{-1}
H_0	Die gap	m

LIST OF FIGURES

LIST OF TABLES

LIST OF APPENDICES

APPENDIX A 1: EXTRUDER AND ANNULAR DIE DETAIL